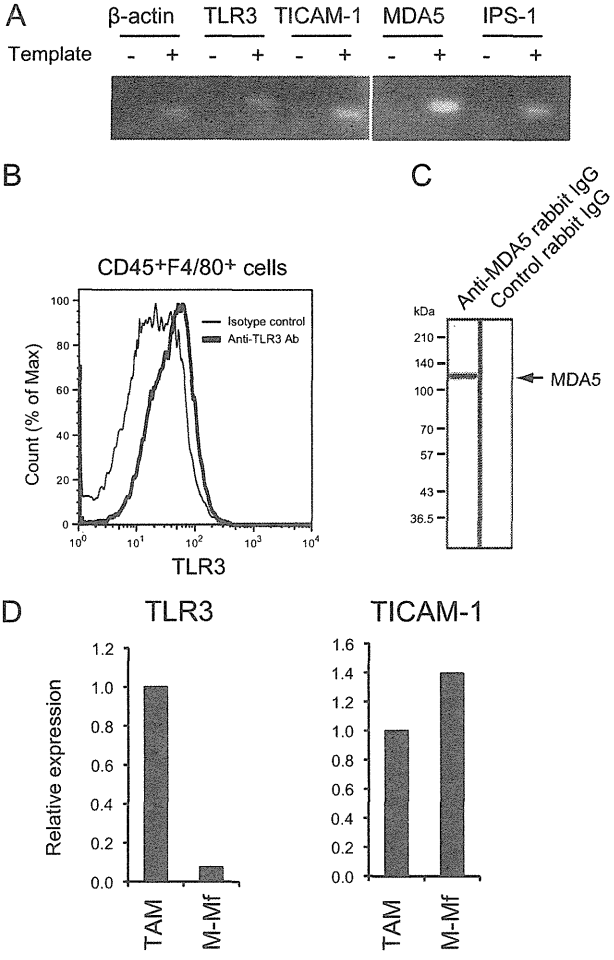

Fig. S10. Expression of TLR3 and MDA5 in 3LL tumor-associated F4/80$^+$ cells. (*A*) mRNA expression of TLR3, TICAM-1, MDA5, and IPS-1 in 3LL tumor-associated F4/80$^+$ cells. Total RNA (1 μg) of F4/80$^+$ cells isolated from 3LL tumor was used as a template for RT-PCR analysis. (*B*) Single-cell suspension of 3LL tumor was stained with FITC-labeled anti-CD45 and PE-labeled anti-F4/80 antibody, followed by intracellular staining with Alexa 647-labeled anti-TLR3 antibody (11F8) or isotype control antibody (rat IgG2a). CD45$^+$F4/80$^+$ cells are shown. (*C*) Cytoplasmic extract of F4/80$^+$ cells was subjected to SDS/PAGE and immunoblotted with rabbit anti-MDA5 antibody or control IgG purified from rabbit serum. (*D*) mRNA expression of TLR3 and TICAM-1 in F4/80$^+$ tumor-associated macrophages (TAM) and macrophage colony-stimulating factor-induced bone marrow-derived macrophages (M-Mf).

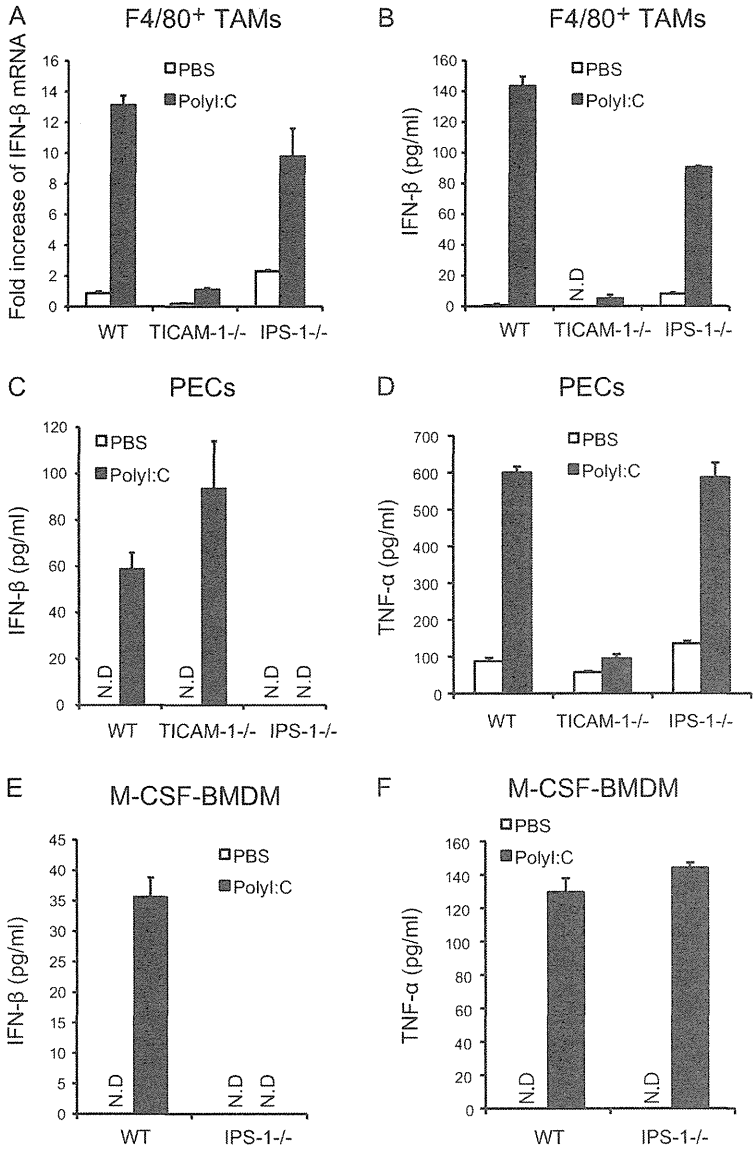

Fig. S11. In vitro stimulation with polyI:C increases the production of IFN-β and TNF-α by Mfs. (*A* and *B*) F4/80$^+$ cells were isolated from 3LL tumor implanted in WT, TICAM-1$^{-/-}$, and IPS-1$^{-/-}$ mice and stimulated with 50 μg/mL polyI:C. After 4 h, cells were harvested and IFN-β mRNA expression was analyzed by quantitative PCR analysis (*A*). After 20 h, IFN-β concentration in culture supernatant was determined by ELISA (*B*). (*C* and *D*) Peritoneal exudate cells (PECs) isolated from WT, TICAM-1$^{-/-}$, and IPS-1$^{-/-}$ mouse were stimulated with 50 μg/mL polyI:C for 20 h. The concentrations of IFN-β (*C*) and TNF-α (*D*) in culture supernatant were determined by ELISA. (*E* and *F*) Macrophage colony-stimulating factor (M-CSF)-induced bone marrow-derived macrophages (BMDM) were prepared from WT and IPS-1$^{-/-}$ mouse and cultured in the presence of 30% L929 supernatant containing M-CSF. After 6 d, adherent cells were harvested and stimulated with 50 μg/mL polyI:C for 20 h. The concentrations of IFN-β (*E*) and TNF-α (*F*) in culture supernatant were determined by ELISA. Data are shown as mean ± SD (n = 3). N.D., not detected. A representative experiment of two with similar outcomes is shown.

Table S1. Expression of various markers on 3LL and MC38 tumor cells

Surface marker	3LL	MC38
H2-K^b	–	++
H2-D^b	±	++
RAE1	++	Not determined
CD45	–	–

Expression of surface markers was analyzed by flow cytometry. Expression was evaluated by mean fluorescence shift: –, ~0.99 ; ±, 1~10 ; +, 11~100 ; ++, 101~.

Table S2. RT-PCR primers used in this study

	Forward primer (5′–3′)	Reverse primer (5′–3′)
IFN-β	CCAGCTCCAAGAAAGGACGA	CGCCCTGTAGGTGAGGTTGAT
IL-12p40	AATGTCTGCGTGCAAGCTCA	ATGCCCACTTGCTGCATGA
IL-6	GTGCATCATCGTTGTTCATACAATC	CTGGGAAATCGTGGAAATGAG
TNF-α	AGGGATGAGAAGTTCCCAAATG	GCTTGTCACTCGAATTTTGAGAAG
IL-1β	TGACGGACCCCAAAAGATGA	TGCTGCTGCGAGATTTGAAG
IL-10	GGCGCTGTCATCGATTTCTC	TGCTCCACTGCCTTGCTCTTA
Cxcl11	GGCTGCGACAAAGTTGAAGTGA	TCCTGGCACAGAGTTCTTATTGGAG
IRF4	AGCCCAGCAGGTTCATAACTACA	CCTCGTGGGCCAAACGT
IRF5	GGTCAACGGGGAAAAGAAACT	CATCCACCCCTTCAGTGTACT
Jmjd3	CGAGTGGTTCGCGGTACAT	GAAGCGGTAAACAGGAATATTGGA
Arg1	GGAATCTGCATGGGCAACCTGTGT	AGGGTCTACGTCTCGCAAGCCA
MMP9	CAAGTGGGACCATCATAACATCA	GATCATGTCTCGCGGCAAGT
VEGFA	GACATCTTCCAGGAGTACC	TGCTGTAGGAAGCTCATCT
Chi3l3	TCACTTACACACATGAGCAAGAC	CGGTTCTGAGGAGTAGAGACCA
Mrc1	CTCTGTTCAGCTATTGGACGC	CGGAATTTCTGGGATTCAGCTTC
Retnla	CCAATCCAGCTAACTATCCCTCC	ACCCAGTAGCAGTCATCCCA
GAPDH	GCCTGGAGAAACCTGCCA	CCCTCAGATGCCTGCTTCA

Table S3. Expression of surface markers on tumor-infiltrated F4/80$^+$ cells

Marker	Expression*
I-Ab	+
H2-D^b	+
H2-K^b	+
CD80	++
CD86	++
CD40	±
CD11c	±
CD3	−
CD4	−
CD8α	−
Gr1	+
B220	+
CD11b	+++
CD206 (MMR)	++

*Expression was evaluated by mean fluorescence shift: −, ~0.99 ; ±, 1 ~10 ; +, 11 ~100 ; ++, 101 ~1,000 ; +++, 1,001~.

JVI
Journals.ASM.org

The Toll-Like Receptor 3-Mediated Antiviral Response Is Important for Protection against Poliovirus Infection in Poliovirus Receptor Transgenic Mice

Yuko Abe,[a] Ken Fujii,[a] Noriyo Nagata,[b] Osamu Takeuchi,[c] Shizuo Akira,[c] Hiroyuki Oshiumi,[d] Misako Matsumoto,[d] Tsukasa Seya,[d] and Satoshi Koike[a]

Neurovirology Project, Tokyo Metropolitan Institute of Medical Science, 2-1-6 Kamikitazawa, Setagaya-ku, Tokyo 156-8506, Japan[a]; Department of Pathology, National Institute of Infectious Diseases, 4-7-1 Gakuen, Musashimurayama, Tokyo 208-0011, Japan[b]; Laboratory of Host Defense, WPI Immunology Frontier Research Center (IFReC), Osaka University, 3-1 Yamada-oka, Suita, Osaka 565-0871, Japan[c]; and Department of Microbiology and Immunology, Hokkaido University Graduate School of Medicine, Kita 15, Nishi 7, Kita-ku, Sapporo 060-8638, Japan[d]

RIG-I-like receptors and Toll-like receptors (TLRs) play important roles in the recognition of viral infections. However, how these molecules contribute to the defense against poliovirus (PV) infection remains unclear. We characterized the roles of these sensors in PV infection in transgenic mice expressing the PV receptor. We observed that alpha/beta interferon (IFN-α/β) production in response to PV infection occurred in an MDA5-dependent but RIG-I-independent manner in primary cultured kidney cells *in vitro*. These results suggest that, similar to the RNA of other picornaviruses, PV RNA is recognized by MDA5. However, serum IFN-α levels, the viral load in nonneural tissues, and mortality rates did not differ significantly between MDA5-deficient mice and wild-type mice. In contrast, we observed that serum IFN production was abrogated and that the viral load in nonneural tissues and mortality rates were both markedly higher in TIR domain-containing adaptor-inducing IFN-β (TRIF)-deficient and TLR3-deficient mice than in wild-type mice. The mortality rate of MyD88-deficient mice was slightly higher than that of wild-type mice. These results suggest that multiple pathways are involved in the antiviral response in mice and that the TLR3-TRIF-mediated signaling pathway plays an essential role in the antiviral response against PV infection.

Poliovirus (PV), which belongs to the genus *Enterovirus* in the family *Picornaviridae*, is the causative agent of poliomyelitis (38). The host range of PV is restricted to primates (18). This species' tropism is determined primarily by the cellular PV receptor (PVR; CD155), which gives the virus access to susceptible cells (14–16, 20). Mice are generally not susceptible to PV. However, transgenic mice expressing human PVR (PVR-tg mice) become susceptible to PV and develop a paralytic disease similar to human poliomyelitis after the administration of PV intravenously, intraperitoneally, intracerebrally, or intramuscularly but not orally (26, 40). PV shows a neurotropic phenotype in both humans and PVR-tg mice. PV preferentially replicates in neurons, especially in motor neurons in the anterior or ventral horn of the spinal cord and in the brainstem. However, the efficiency of PV replication is low in nonneural tissues (4, 25). We previously found that innate immune responses that are mediated by type I interferons (IFNs) play important roles in controlling viral replication in nonneural tissues and in the mortality rates of PVR-tg mice (19). In PVR-tg mice deficient in IFNAR1, PV efficiently replicates in nonneural tissues such as the liver, pancreas, and spleen, which are not normal targets of PV. IFNAR1-deficient mice die after the inoculation of a small amount of PV by peripheral routes. The results suggest that the type I IFN response forms an innate immune barrier that prevents PV replication in nonneural tissues and subsequent PV invasion of the central nervous system (CNS). This response therefore plays important roles in the tissue tropism and pathogenicity of PV (25).

The sensors that are involved in the production of type I IFNs in response to RNA viral infections have been recently identified and characterized (1, 46–48). The RIG-I-like receptors (RLRs) retinoic-acid-inducible gene 1 (RIG-I) and melanoma differentiation-associated gene 5 (MDA5) are expressed in the cytoplasm of all cell types, with the exception of plasmacytoid dendritic cells (pDCs). RIG-I and MDA5 have RNA binding domains and differentially recognize specific characteristics of nonself viral RNAs (17, 22, 36, 37). In addition, RLRs have DExD/H box RNA helicase domains (51) that activate downstream signaling pathways resulting in the activation of IFN regulatory factor 3 (IRF-3) and IRF-7 (53). TLR3 and TLR7 are the sensors for viral double-stranded RNA (dsRNA) and single-stranded RNA, respectively (2, 8, 12). TLR3 is expressed in the endosome of macrophages and conventional dendritic cells (DCs) (28) but not in pDCs. TLR3 is also expressed in a variety of epithelial cells, including airway, uterine, corneal, vaginal, cervical, biliary, and intestinal epithelial cells, which may function as efficient barriers to infection. The TLR3-mediated signaling pathway is transmitted through Toll–interleukin-1 (IL-1) receptor (TIR)-containing adaptor molecule 1, which is also known as TIR domain-containing adaptor inducing IFN-β (TRIF), and finally results in the activation of IRF3 and IRF7 (13, 34, 51). TLR7 is specifically expressed in the endosome of pDCs and contributes to the production of a large amount of IFNs in response to many RNA virus infections (5, 7). TLR7 signaling is mediated by the adaptor molecule myeloid differentiation factor 88 (MyD88). These sensors do not contribute equally

Received 29 May 2011 Accepted 20 October 2011
Published ahead of print 9 November 2011
Address correspondence to Satoshi Koike, koike-st@igakuken.or.jp.

doi:10.1128/JVI.05245-11

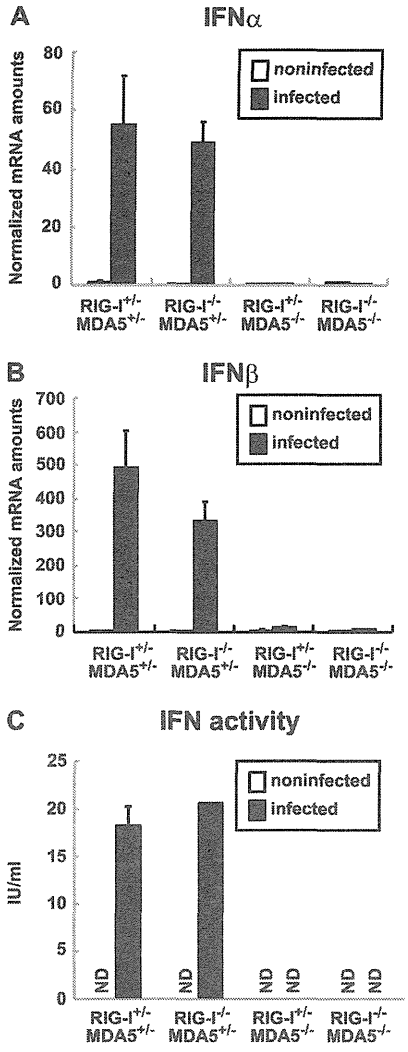

FIG 1 Production of IFNs in primary cultured kidney cells prepared from RIG-I- and MDA5-deficient mice. Kidney cells were pretreated with 100 U of IFN-β for 2 h and infected with PV at an MOI of 10. RNA was prepared from the infected cells at 6 hpi. The amounts of IFN-α mRNA (A) and IFN-β mRNA (B) were determined using quantitative real-time PCR. Cells were prepared in duplicate, and the experiments were repeated three times. Representative data are shown. The amount of IFN activity in the supernatant of infected kidney cells at 8 hpi was determined by the cytopathic effect dye uptake method using L929 cells (C). ND, not detected.

to the antiviral response to each viral infection. The type I IFN production that is induced by these sensors occurs in a virus-specific and cell-specific manner (21, 23). For example, RIG-I plays an important role in the antiviral response to Newcastle disease virus, influenza A virus, Sendai virus, vesicular stomatitis virus, Japanese encephalitis virus, and hepatitis C virus. However, MDA5 is important in the response to infection with picornaviruses, such as encephalomyocarditis virus (EMCV) (10, 23). Although RNA viruses produce dsRNA during the replication step, the protective effect of the TLR3-mediated pathway is not clear (9). In a previous study, TLR3 expression was found to cause severe encephalitis in West Nile virus (WNV) infection (50). How these sensor molecules contribute to the recognition of PV infection is not understood. The aim of the present study was to determine the role of these sensors in the response to PV infection in transgenic mice expressing human PVR. We generated PVR-tg mice deficient in these sensor and adaptor molecules. Our results demonstrate that the MDA5-, TRIF- and MyD88-mediated pathways contribute to the antiviral response against PV infection and that the TLR3-TRIF-mediated pathway plays a pivotal role in this response.

MATERIALS AND METHODS

Cells and viruses. An AGMK cell line, JVK-03 (24), was maintained in Eagle's minimum essential medium containing 5% fetal bovine serum. PV type I Mahoney, a strain derived from the infectious cDNA clone pOM, was used in this study (45). The virus was propagated in JVK-03, and the viral titer was determined using the plaque assay. Primary cultured kidney cells were prepared from transgenic and knockout mice as previously described (54).

Transgenic and knockout mice and infection experiments. All experiments using mice were performed in accordance with the Guidelines for the Care and Use of Laboratory Animals of the Tokyo Metropolitan Institute of Medical Science. ICR-PVRTg21 mice (26) were mated with RIG-I$^{-/-}$ and/or MDA5$^{-/-}$ mice (21) in the ICR background because it is difficult to maintain RIG-I$^{-/-}$ mice in other genetic backgrounds. We mated mice and obtained littermates with the genotypes RIG-I$^{+/-}$ MDA5$^{+/-}$, RIG-I$^{-/-}$ MDA5$^{+/-}$, RIG-I$^{+/-}$ MDA5$^{-/-}$, and RIG-I$^{-/-}$ MDA5$^{-/-}$ to use in experiments. C57BL/6 (B6)-PVRTg21 mice were mated with MDA5$^{-/-}$ mice, TRIF$^{-/-}$ mice, MyD88$^{-/-}$ mice, and TLR3$^{-/-}$ mice (51) in the B6 background (backcrossed 7 to 10 times). IFNAR1$^{-/-}$ PVR-tg mice were previously described (19). Because all of the mice that were used in the present study were in the PVR-tg background, we omitted the notation "PVR-tg" for simplicity in this report. Six- to 7-week-old mice were used for infection experiments. The survival and clinical symptoms of the mice were observed daily for 3 weeks. At the first sign of severe neurological symptoms, the mice were sacrificed as a humane endpoint.

Measurement of IFN levels. IFN-α levels in the sera were determined using an enzyme-linked immunosorbent assay (ELISA). The ELISA kit for IFN-α was purchased from PBL Biochemical Laboratories. Mouse IFN activity in the supernatants of PV-infected kidney cells was measured by the cytopathic effect dye uptake method using L929 cells (54, 55). Recombinant mouse IFN-β (Toray) was used as the standard for unit definition.

Quantitative real-time reverse transcription (RT)-PCR. RNA was isolated from the tissues of infected mice or infected cells using the Isogen RNA extraction kit (Nippon Gene). DNase I treatment and cDNA synthesis were performed as previously described (54). The amounts of the mRNAs for IFN-α, IFN-β, OAS1a, and IRF-7 were determined using real-time RT-PCR with an ABI Prism 7500 (Applied Biosystems) as previously described (54).

RESULTS

IFN production in primary cultured kidney cells is dependent on MDA5. We examined whether, similar to EMCV infection, PV infection is recognized by MDA5 *in vitro*. We mated PVR-tg mice with MDA5-deficient and RIG-I-deficient mice to generate RIG-I$^{+/-}$ MDA5$^{+/-}$, RIG-I$^{-/-}$ MDA5$^{+/-}$, RIG-I$^{+/-}$ MDA5$^{-/-}$, and RIG-I$^{-/-}$ MDA5$^{-/-}$ mice in the ICR background. We prepared primary cultured kidney cells from mice with these genotypes to determine the role of RLRs. After cultivation for approximately 1 week, the cells that became confluent were infected with PV at a multiplicity of infection (MOI) of 10. RNA was recovered from the infected cells at 6 hpi, and the amounts of the mRNAs for IFN-α and IFN-β were determined using real-time RT-PCR. Kid-

ney cells that were not pretreated with IFN-β before PV infection showed rapid cytopathic effect progression and did not produce IFN mRNA (data not shown). This result is consistent with our previous observations (54). We therefore pretreated cells with 100 U of IFN-β for 2 h and infected them with PV. As we reported previously, the IFN-treated kidney cells became resistant to PV infection, PV replication was severely inhibited, and IFN production was observed (54). Under this condition, we determined the sensor responsible for IFN production. We observed the induction of both IFN-α (Fig. 1A) and IFN-β mRNAs (Fig. 1B) in cells that were isolated from RIGI-I$^{+/-}$ MDA5$^{+/-}$ mice and RIGI-I$^{-/-}$ MDA5$^{+/-}$ mice but not from RIGI-I$^{+/-}$ MDA5$^{-/-}$ mice or RIGI-I$^{-/-}$ MDA5$^{-/-}$ mice. The induced IFN proteins were not detected by ELISA due to a very small amount of IFNs produced in the supernatants. However, IFN activity was detected in the supernatants of PV-infected kidney cells prepared from RIGI-I$^{+/-}$ MDA5$^{+/-}$ mice and RIGI-I$^{-/-}$ MDA5$^{+/-}$ mice but not from RIGI-I$^{+/-}$ MDA5$^{-/-}$ mice or RIGI-I$^{-/-}$ MDA5$^{-/-}$ mice using the cytopathic effect dye uptake method (Fig. 1C). These results suggest that PV infection is recognized by MDA5 but not RIG-I in primary murine kidney cells, which is consistent with previous reports demonstrating that MDA5 is essential for the detection of picornaviruses (10, 23). However, MDA5-mediated IFN production was observed only when cells had been primed with a low dose of IFNs.

IFN responses of MDA5-deficient mice are not significantly different from those of wild-type mice. We hypothesized that MDA5 plays an important role in the type I IFN response upon PV infection *in vivo*. We examined the serum IFN-α levels in PVR-tg mice intravenously infected with 2×10^7 PFU of PV using ELISA. Their serum IFN-α level was initially observed at 9 hpi, peaked at 12 hpi, and began to decline at 24 hpi (Fig. 2A). We then determined the serum IFN-α levels of the knockout mice at 12 hpi. Unexpectedly, similar serum IFN-α levels were detected in RIG-I$^{+/-}$ MDA5$^{+/-}$, RIG-I$^{+/-}$ MDA5$^{-/-}$, RIG-I$^{-/-}$ MDA5$^{+/-}$, and RIG$^{-/-}$ MDA5$^{-/-}$ mice infected with PV (Fig. 2B).

We monitored the induction of mRNAs for the IFN-stimulated genes (ISGs), OAS1a (Fig. 3A) and IRF-7 (Fig. 3B), in the brain, spinal cord, liver, spleen, and kidney using real-time RT-PCR. Among the organs tested, the expression levels of these ISGs were the highest in the spleen. However, the expression profiles of these genes were essentially the same in all organs. In accordance with the elevated serum IFN levels, the induction of ISGs in various organs was observed in all mice (Fig. 3A and B). The results suggest that MDA5 does not play a critical role in IFN production and subsequent ISG induction in response to PV infection *in vivo*.

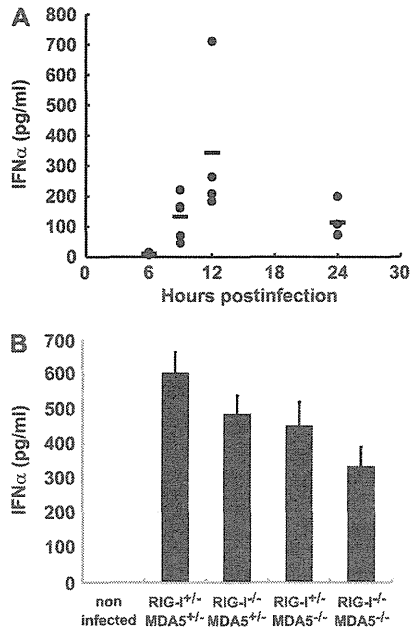

FIG 2 Production of serum IFN-α in RIG-I- and MDA5-deficient mice. (A) Time course of IFN-α levels in serum. PVR-tg mice in the B6 background (n = 4 or n = 5) were intravenously infected with 2×10^7 PFU of PV. Serum samples were collected at the indicated time points, and the concentration of IFN-α was determined using ELISA. (B) IFN-α levels of RIG-I- and MDA5-deficient mice in the ICR background (n = 8) at 12 hpi were compared. The experiments were repeated twice, and representative data are shown.

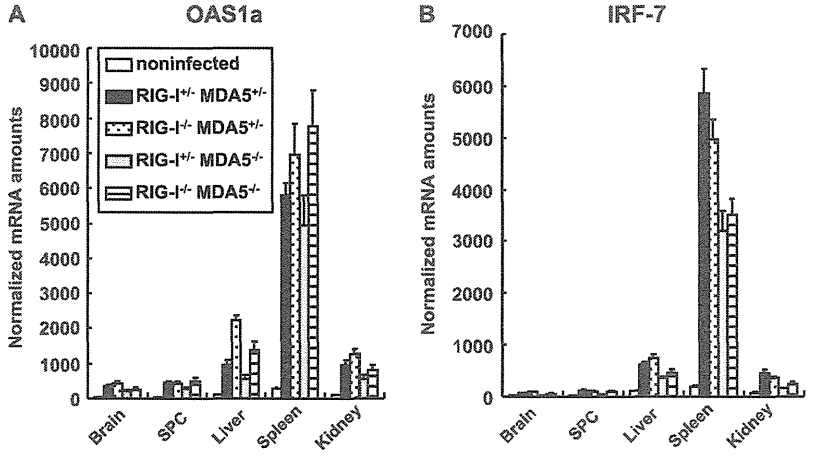

FIG 3 ISG induction in RIG-I- and MDA5-deficient mice. Mice (n = 4) were intravenously infected with 2×10^7 PFU of PV. At 12 hpi, RNA was isolated from the indicated tissues of the infected mice and OAS1a (A) and IRF-7 (B) mRNA levels were determined using quantitative real-time PCR. The experiments were repeated twice, and representative data are shown. SPC, spinal cord.

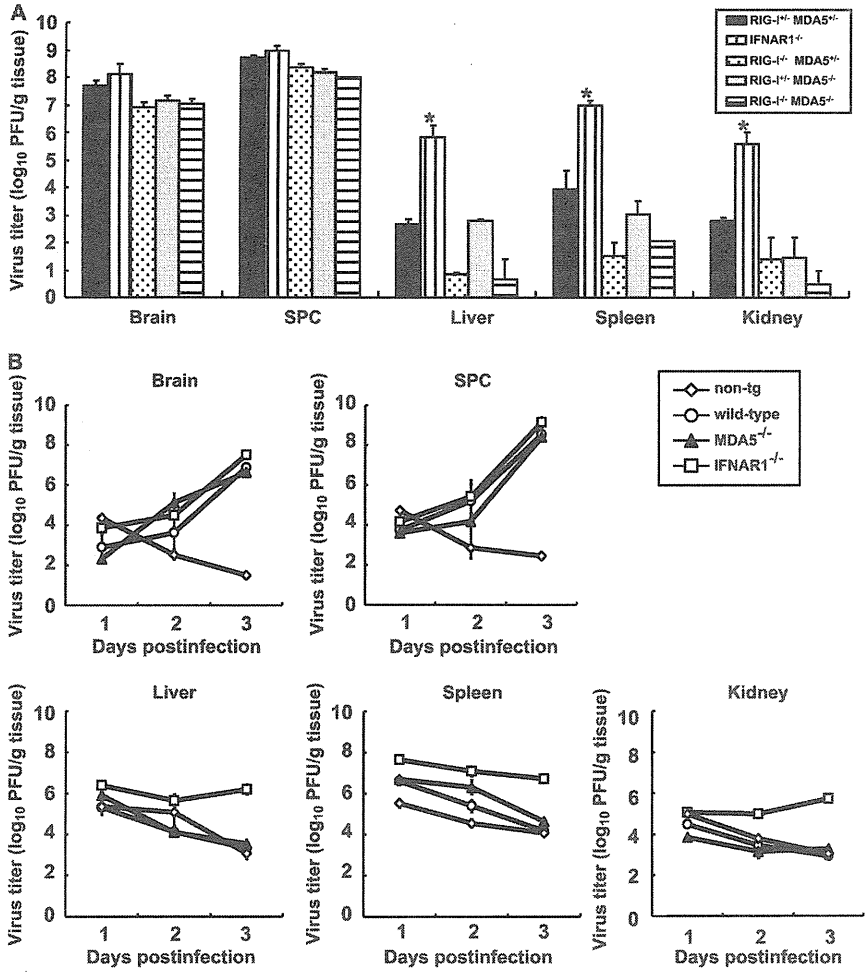

FIG 4 (A) PV replication in RIG-I- and MDA5-deficient mice. RIGI-$I^{+/-}$ $MDA5^{+/-}$, RIGI-$I^{-/-}$ $MDA5^{+/-}$, RIGI-$I^{-/-}$ $MDA5^{+/-}$, and RIGI-$I^{-/-}$ $MDA5^{-/-}$ mice in the ICR background and $IFNAR1^{-/-}$ mice in the B6 background ($n = 3$) were intravenously infected with 2×10^7 PFU of PV. Infected mice were paralyzed or dead at 3 to 5 days postinfection. The tissues of the paralyzed mice were collected, and the viral titers were determined using a plaque assay (*, $P < 0.01$ by t test compared to RIGI-$I^{+/-}$ $MDA5^{+/-}$ mice). (B) PV replication kinetics in MDA5-deficient mice. Nontransgenic (non-tg) mice, wild-type mice, $MDA5^{-/-}$ mice, and $IFNAR1^{-/-}$ mice in the B6 background ($n = 3$) were infected as described above. Tissues were collected daily, and viral titers were determined. SPC, spinal cord.

PV replication in nonneural tissues and mortality rates of mice deficient in RIG-I-like receptors. We have previously shown that the IFN-α/β response forms an innate immune barrier to prevent PV replication in nonneural tissues and PV invasion of the CNS (19, 25). Therefore, we evaluated PV replication in neural and nonneural tissues in RLR-deficient mice. The mice were infected with 2×10^7 PFU of PV, which is approximately 100 times higher than the 50% lethal doses for all mouse strains. The infected mice showed paralysis by 3 to 5 days postinfection. The brain, spinal cord, liver, spleen, and kidney of the paralyzed mice were recovered, and their viral titers were determined (Fig. 4A). PV was recovered from the CNS of the paralyzed mice almost equally among the genotypes. The viral titers recovered from the liver, spleen, and kidney of $IFNAR1^{-/-}$ mice were significantly higher than those of wild-type mice, as previously described (19). However, PV titers that were recovered from these organs of RIG-$I^{-/-}$ $MDA5^{+/-}$, RIG-$I^{+/-}$ $MDA5^{-/-}$, and RIG-$I^{-/-}$ $MDA5^{-/-}$ mice were as low as or lower than those in the organs of RIG-$I^{+/-}$ $MDA5^{+/-}$ mice. We then examined virus replication kinetics using nontransgenic mice, wild-type mice, $IFNAR^{-/-}$ mice, and $MDA5^{-/-}$ mice in the B6 background (Fig. 4B). The viral load in the CNS increased in a similar fashion among the transgenic mouse strains. However, the viral load kinetics in the liver, spleen, and kidney of wild-type and $MDA5^{-/-}$ mice were similar to those of nontransgenic mice. The values for nontransgenic mice indicate the kinetics of clearance of inoculated virus. The results indicated that PV replication was severely inhibited in the liver, spleen, and kidney of wild-type and $MDA5^{-/-}$ mice. This inhibition correlated well with the induction of serum IFNs in $MDA5^{-/-}$ mice (Fig. 2). The PV antigen was detected in neurons in the CNS but not in other tissues in all knockout mice (Table 1). This result indicates that the lack of RLRs did not alter the tissue tropism of PV. These data suggest that inhibition of PV replication in nonneural tissues is not dependent on RLRs and that MDA5-independent mechanisms are the major contributors in controlling PV replication.

We examined the mortality rates of RIG-$I^{+/-}$ $MDA5^{+/-}$, RIG-$I^{-/-}$ $MDA5^{+/-}$, RIG-$I^{+/-}$ $MDA5^{-/-}$, and RIG-$I^{-/-}$ $MDA5^{-/-}$

TABLE 1 PV antigens in RIG-I- and MDA5-deficient mice

Organ or tissue	No. of PV antigen-positive mice/no. of mice tested			
	RIG-I$^{+/-}$ MDA5$^{+/-}$	RIG-I$^{-/-}$ MDA5$^{+/-}$	RIG-I$^{+/-}$ MDA5$^{-/-}$	RIG-I$^{-/-}$ MDA5$^{-/-}$
Brain	4/4	3/3	4/4	4/4
Spinal cord	4/4	3/3	4/4	4/4
Heart	0/4	0/3	0/4	0/4
Lung	0/4	0/3	0/4	0/4
Liver	0/4	0/3	0/4	0/4
Kidney	0/4	0/3	0/4	0/4
Spleen	0/4	0/3	0/4	0/4
Pancreas	0/4	0/3	0/4	0/4
Intestine	0/4	0/3	0/4	0/4
Adipose tissue	0/4	0/3	0/4	0/4

mice in the ICR background after intravenous infection with PV at 10^3, 10^4, and 10^5 PFU (Fig. 5A, B, and C). The mortality rates of these mice did not differ significantly from each other. We observed that the mortality rates of RIG-I$^{+/-}$ MDA5$^{-/-}$ mice that were inoculated with 10^4 PFU of PV was slightly higher than the mice of other genotypes. However, significant differences were not observed in mice that were inoculated with the other doses. Similar experiments were performed using MDA5$^{-/-}$ and MDA5$^{+/-}$ mice in the B6 background (Fig. 5D, E, and F). We did not observe significant differences between the MDA5$^{-/-}$ and MDA5$^{+/-}$ mice. The mortality rate of MDA5$^{-/-}$ mice was slightly higher than that of MDA5$^{+/-}$ mice that were inoculated with 10^5 PFU of PV. However, the opposite trend was observed when mice

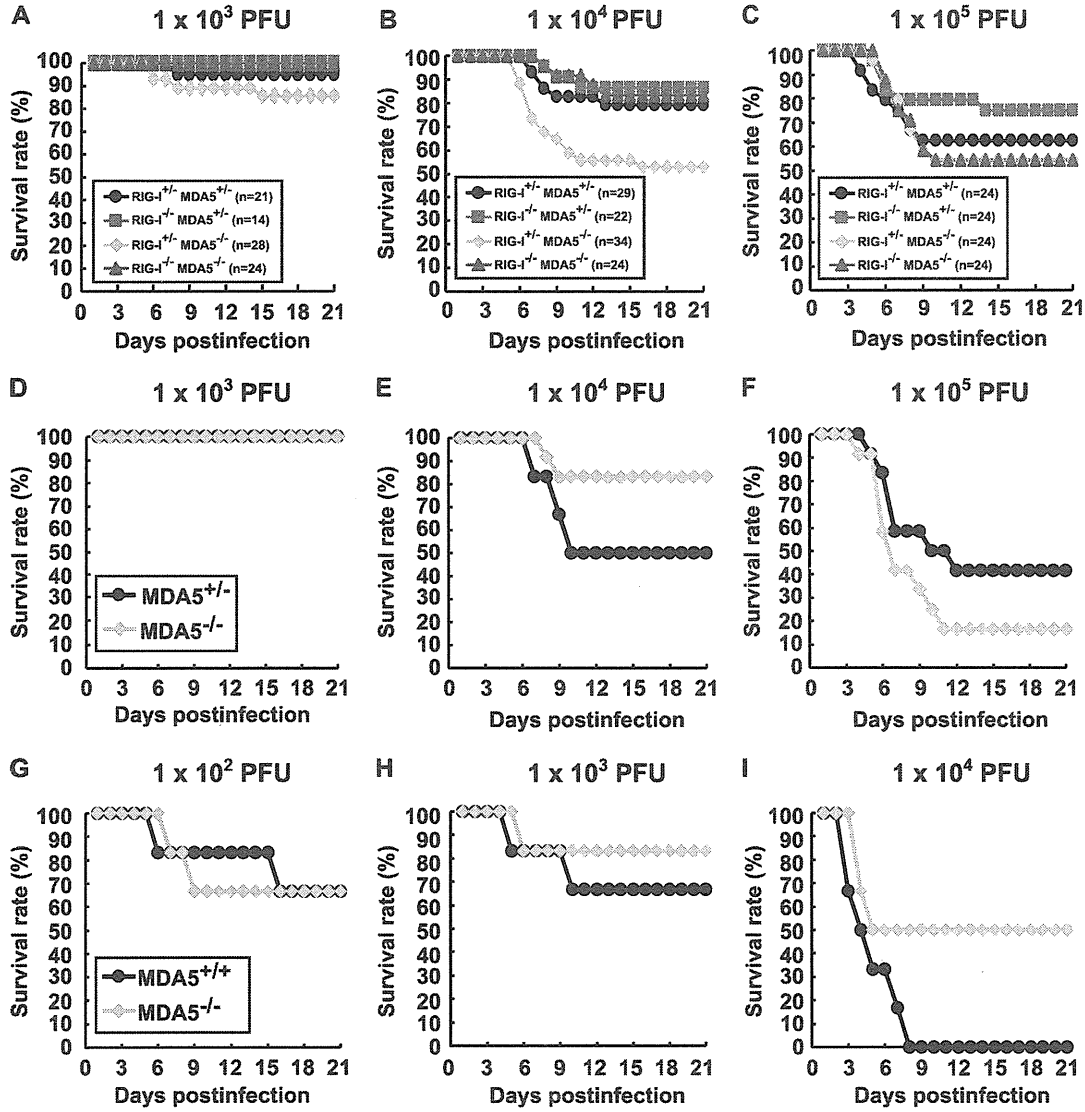

FIG 5 Mortality rates of RIG-I- and MDA5-deficient mice. Littermates of the genotypes indicated were obtained by mating RIGI-I$^{+/-}$ MDA5$^{+/-}$ and RIGI-I$^{-/-}$ MDA5$^{-/-}$ mice in the ICR background. The mice were infected intravenously with 10^3 (A), 10^4 (B), or 10^5 (C) PFU of PV. The results shown are the sums of several independent experiments. The total numbers of mice of the different genotypes that were used are boxed, and the doses used are shown at the top. Littermates of MDA5$^{+/-}$ and MDA5$^{-/-}$ mice were obtained in the B6 background. The mice (n = 12) were intravenously infected with 10^3 (D), 10^4 (E), or 10^5 (F) of PV. MDA5$^{+/+}$ and MDA5$^{-/-}$ mice (n = 6) were intracerebrally infected with 10^2 (G), 10^3 (H), or 10^4 (I) PFU of PV, respectively. We monitored the survival rates of the mice for 3 weeks after infection.

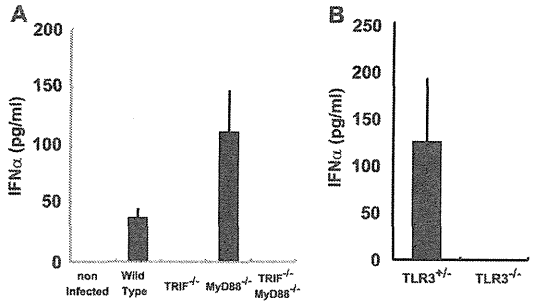

FIG 6 Production of serum IFN-α in TRIF-, MyD88-, and TLR3-deficient mice. Mice (n = 3 or 8) were intravenously infected with 10^7 PFU of PV. IFN-α levels of TRIF- and MyD88-deficient mice (A) and TLR3-deficient mice (B) at 12 hpi were compared. The experiments were repeated twice, and representative data are shown.

were inoculated with 10^4 PFU of PV. We suspect that the slight difference between the mortality rates of wild-type and MDA5$^{-/-}$ mice was in the range of experimental fluctuation, and thus, the disruption of MDA5 did not significantly influence the mortality rate. In order to determine if the same is true when mice are infected by other routes, we inoculated wild-type and MDA5$^{-/-}$ mice with PV intracerebrally and compared their mortality rates (Fig. 5G to I). Their mortality rates did not differ significantly. These results suggest that MDA5 does not make a great contribution to the protection of mice, at least after intracerebral and intravenous infections. Taken together, the MDA5-mediated response does not play a dominant role in IFN production, ISG induction, or inhibition of PV replication *in vivo*, unlike the MDA5-mediated effects on EMCV infection.

IFN response in TRIF- and MyD88-deficient mice. Because the experiments with MDA5-deficient mice suggested the existence of other protective mechanisms in PV infection, we investigated the role of TLRs using TRIF- and MyD88-deficient mice. PVR-tg mice were mated with TRIF$^{-/-}$ and/or MyD88$^{-/-}$ mice in the B6 background. Serum IFN-α of mice infected with 10^7 PFU of PV was measured using ELISA at 12 hpi (Fig. 6A). Interestingly, serum IFN production in response to PV infection was abrogated in TRIF$^{-/-}$ mice. Because TRIF acts as an adaptor for TLR3 and TLR4, we tested whether the same phenomenon occurs in TLR3$^{-/-}$ mice. Serum IFN induction was not observed in TLR3-deficient mice (Fig. 6B). These results suggest that the TLR3-mediated pathway is essential for IFN production in response to PV infection.

We next assessed the induction of mRNAs for OAS1a (Fig. 7A) and IRF-7 (Fig. 7B) in various organs using real-time RT-PCR. The induction of OAS1a and IRF-7 was observed in all mice. Although serum IFN production was abrogated in TRIF$^{-/-}$ mice and TRIF$^{-/-}$ MyD88$^{-/-}$ mice (Fig. 6), a significant level of ISG mRNA was induced. However, the induction levels were slightly lower than those in wild-type mice in some cases. The results suggest that the TRIF-mediated pathway contributes to ISG expression mainly through the induction of serum IFNs in response to PV infection and that some other mechanisms may also contribute to ISG expression.

PV replication in nonneural tissues and mortality rates of TRIF- and MyD88-deficient mice. The brain, spinal cord, liver, spleen, and kidney of paralyzed mice were recovered, and viral titers were determined (Fig. 8). PV was recovered from the CNS of TRIF$^{-/-}$, MyD88$^{-/-}$, and TLR3$^{-/-}$ mice, and the titers were not different from those of wild-type mice. However, the viral titers of the liver, spleen, and kidney of TRIF$^{-/-}$ and TLR3$^{-/-}$ mice were significantly higher than those of wild-type mice but lower than those of IFNAR1$^{-/-}$ mice. We then examined the virus replication kinetics in TRIF$^{-/-}$ mice (Fig. 8B). The viral load in the CNS increased in TRIF$^{-/-}$ mice similarly to that in other mice. In accordance to the absence of serum IFN (Fig. 2), the viral loads in the liver, spleen, and kidney of TRIF$^{-/-}$ mice increased, while the viral loads in these organs of wild-type mice decreased. PV antigens were detected in the CNS of all of the knockout mice. In addition, PV antigens were detected in the adipose tissue, pancreas, and kidney of several TRIF$^{-/-}$ and MyD88$^{-/-}$ mice (Table 2). These results suggest that these tissues support viral multiplication in these knockout mice and that the TLR-mediated signaling pathways contribute to the regulation of PV replication in nonneural tissues.

The mortality rates of TRIF$^{-/-}$, MyD88$^{-/-}$, and TLR3$^{-/-}$

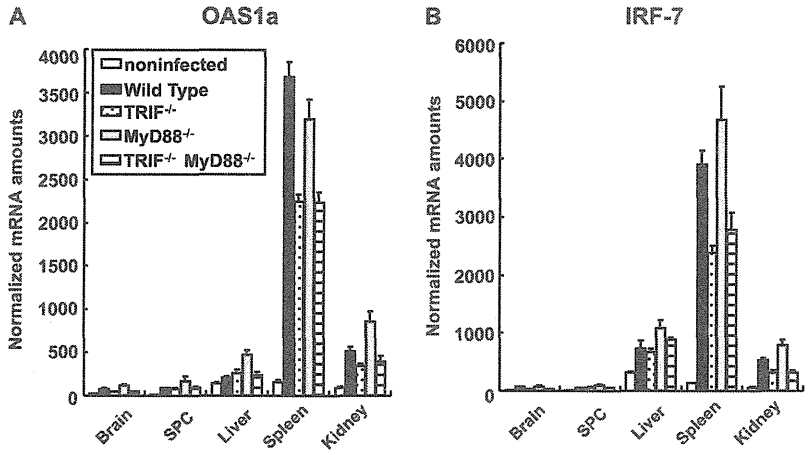

FIG 7 ISG induction in TRIF- and MyD88-deficient mice. Mice (n = 4) were intravenously infected with 10^7 PFU of PV. At 12 hpi, RNA was isolated from the indicated tissues of the infected mice and OAS1a (A) and IRF-7 (B) mRNA levels were determined by quantitative real-time PCR. The experiments were repeated twice, and representative data are shown. SPC, spinal cord.

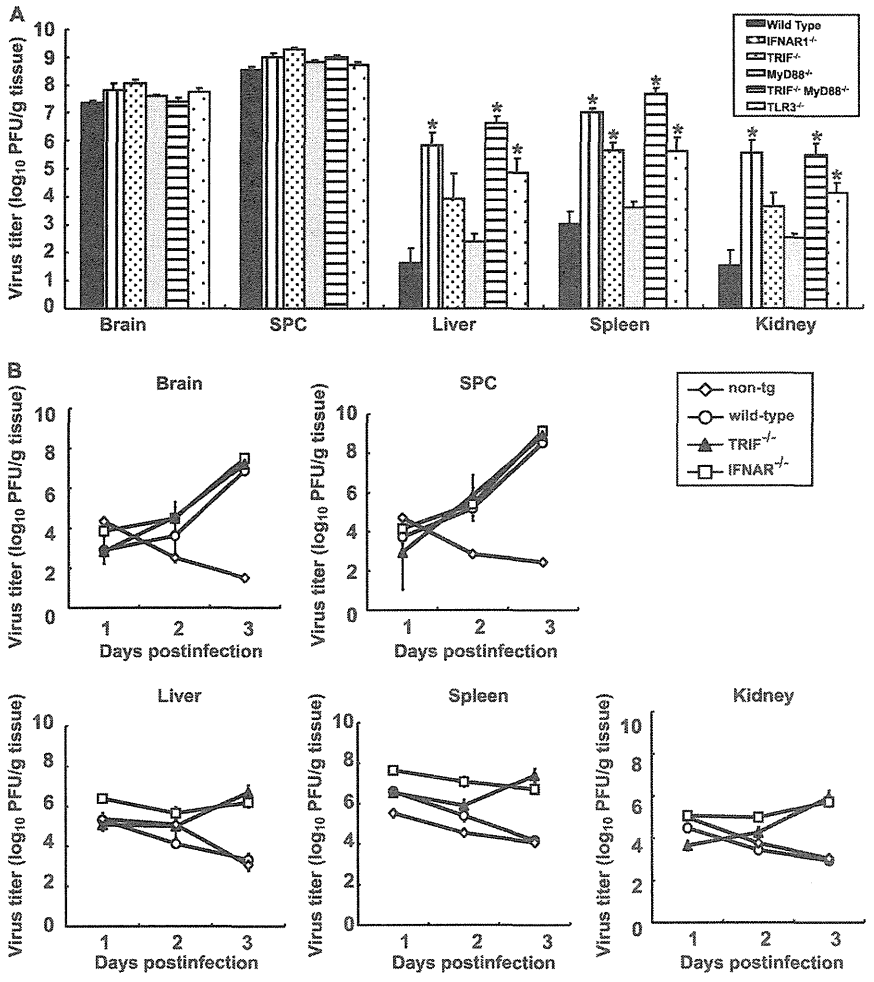

FIG 8 (A) PV replication in TRIF- and MyD88-deficient mice. Wild-type ($n = 4$), TRIF$^{-/-}$ ($n = 4$), MyD88$^{-/-}$ ($n = 6$), TRIF$^{-/-}$ MyD88$^{-/-}$ ($n = 4$), TLR3$^{-/-}$ ($n = 5$), and IFNAR1$^{-/-}$ ($n = 4$) mice were intravenously infected with 10^7 PFU of PV. The infected mice were paralyzed or dead at 3 to 5 days postinfection. The indicated tissues were collected, and viral titers were determined using a plaque assay (*, $P < 0.01$ by t test compared to wild-type mice). (B) PV replication kinetics in TRIF-deficient mice. Nontransgenic mice, wild-type mice, TRIF$^{-/-}$ mice, and IFNAR1$^{-/-}$ mice ($n = 3$) were infected as described above. Tissues were collected daily, and viral titers were determined. The results for nontransgenic (non-tg) mice, wild-type mice, and IFNAR1$^{-/-}$ mice are the same as those in Fig. 4B. SPC, spinal cord.

TABLE 2 PV antigens in TRIF- and MyD88-deficient mice

Organ or tissue	No. of PV antigen-positive mice/no. of mice tested			
	Wild type	TRIF$^{-/-}$	MyD88$^{-/-}$	TRIF$^{-/-}$ MyD88$^{-/-}$
Brain	6/6	8/8	9/9	6/6
Spinal cord	6/6	8/8	9/9	6/6
Heart	0/6	0/8	0/8	0/6
Lung	0/6	0/8	0/8	0/6
Liver	0/6	0/8	0/9	0/6
Kidney	0/6	0/8	2/9	0/5
Spleen	0/6	0/8	0/9	0/6
Pancreas	2/6	0/8	7/9	4/6
Intestine	0/6	0/8	0/9	0/6
Adipose tissue	0/6	2/8	2/9	3/6

mice were compared (Fig. 9). Approximately 25% of the TRIF$^{-/-}$ mice died after infection with 10^2 PFU of PV, and almost all of the mice died after infection with more than 10^3 PFU of PV (Fig. 9A). Approximately 20% and 60% of the MyD88$^{-/-}$ mice died after infection with 10^3 and 10^4 PFU of PV, respectively (Fig. 9B and C). TRIF$^{-/-}$ MyD88$^{-/-}$ mice were the most susceptible. In total, 70% of the mice died after infection with 10^2 PFU of PV (Fig. 9A). The mortality rate of TRIF$^{-/-}$ MyD88$^{-/-}$ mice was very close to that of IFNAR1$^{-/-}$ mice (19). The mortality rate of TLR3$^{-/-}$ mice was similar to that of TRIF$^{-/-}$ mice (Fig. 9D, E, and F). These results suggest that the TRIF-mediated and MyD88-mediated antiviral responses contribute to the host's defense against PV infection and that the TLR3-TRIF-mediated response has the most dominant effect.

DISCUSSION

Each virus infects different cell types and has a characteristic mode of replication. In mammalian hosts, several viral RNA sensors,

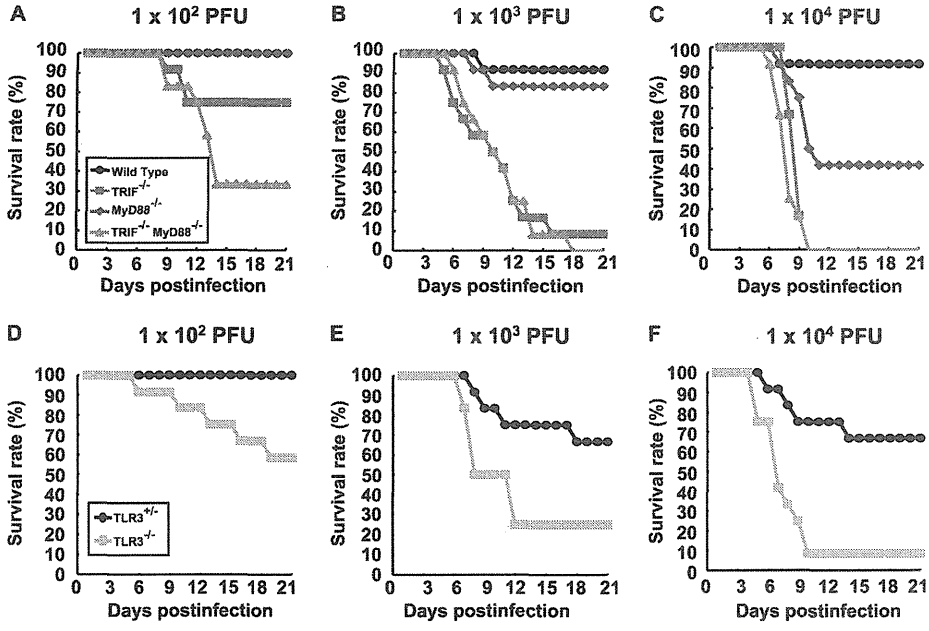

FIG 9 Mortality rates of TRIF-, MyD88-, and TLR3-deficient mice. (A) Wild-type, TRIF$^{-/-}$, MyD88$^{-/-}$, and TRIF$^{-/-}$ MyD88$^{-/-}$ mice (n = 12) were intravenously inoculated with the indicated doses of PV. (B) Littermates of TLR3$^{+/-}$ and TLR3$^{-/-}$ mice (n = 12) were used.

which are expressed in different cell types and recognize different molecular patterns, have evolved to counteract a variety of viruses. In the present study, we demonstrated that the MDA5-, TRIF-, and MyD88-mediated pathways contribute to the recognition of PV infection and that the TLR3-TRIF-mediated pathway plays the most important role in the antiviral response. Since all of the phenotypes shown after PV infection in the TRIF$^{-/-}$ mice and TLR3$^{-/-}$ mice are very similar to each other, we think that the contribution of the TLR3-mediated response is dominant and that of the TLR4-mediated response is negligible.

Previous reports have revealed that IFN is produced efficiently in EMCV-infected fibroblasts in an MDA5-dependent manner and that MDA5 contributes to the induction of serum IFNs and the protection of mice against EMCV (10, 23). Because EMCV belongs to the family *Picornaviridae*, we hypothesized that MDA5 also contributes to IFN induction in response to PV infection. However, the MDA5-dependent pathway did not play a dominant role in the defense against PV infection. Therefore, we speculate that PV uses mechanisms different from those of EMCV to strongly suppress IFN production *in vivo*. Indeed, IFN production in cultured cells in response to PV infection was observed only when the cells were pretreated with a low dose of IFNs. In addition, the amount of IFN produced was much lower than that produced in response to EMCV infection (Fig. 1). This result suggests that IFN induction in infected cells is suppressed and that this PV-mediated effect may be stronger than that of EMCV. Translational shutoff may be one of the reasons for this difference. PV 3A protein causes a change in membrane trafficking that prevents protein secretion and may also contribute to the suppression of IFN production (6). Caspase-dependent cleavage of MDA5 (3) and IPS-1 (39) in PV-infected cells has been reported. Through these possible mechanisms, PV may induce the suppression of IFN production in mice *in vivo*, and the MDA5-mediated pathway does not play an essential role in the host response, unlike in EMCV infection. PV and EMCV seemed to use different strategies to counteract the host innate immune system, even though PV and EMCV belong to the same family. Thus, TLR3 became the sensor that functions most effectively for PV as a result of PV evolution. Although the TLR3-TRIF-mediated pathway plays a dominant role, the fact that significant ISG induction was observed in PV-infected TRIF$^{-/-}$ and TRIF$^{-/-}$ MyD88$^{-/-}$ mice (Fig. 7) suggested that other mechanisms also operate in combination with this pathway.

The viral loads in the nonneural tissues of TLR3- and TRIF-deficient mice were much higher than those in wild-type mice, whereas the viral loads in the CNS were not significantly different in paralyzed mice (Fig. 8). These results suggest that the TLR3-TRIF-mediated pathway inhibits viral replication mainly before viral invasion of the CNS rather than after invasion and that this response plays an important role in preventing the viral invasion of the CNS. In the CNS, replication of PV was not effectively inhibited, even in wild-type mice. This result is consistent with our previous results obtained using IFNAR1$^{-/-}$ mice and suggests that the antivirus response in the CNS is different from that in nonneural tissues upon PV infection (19). The cell tropism of PV may influence the efficiency of the immune response. For example, if PVR is expressed in TLR3-expressing cells, then PV replication would be detected immediately after infection. Alternatively, if PV infection *in vivo* occurs in the vicinity of TLR3-expressing immune cells such as DCs and macrophages, PV-infected cells may readily be captured by TLR3-expressing cells, thereby facilitating efficient cross-priming (27, 44) of PV RNA. PV infects neurons almost exclusively and not other cell types in the CNS. If neurons do not have the ability to induce a strong TLR3-mediated antiviral response upon PV infection, the CNS may be more defective in the innate immune response than nonneural tissues are. This may be one of the reasons why PV replicates preferentially in the CNS. Further studies on PV pathogenesis related to the innate

immune response will make a great contribution to elucidating the mechanisms of PV tissue tropism.

TLR3 recognizes dsRNA. However, the protective role of TLR3 in the response to many RNA viral infections is not clear (9, 29, 43). A previous study has demonstrated that WNV, which is an encephalitis virus belonging to the family *Flaviviridae*, causes more severe encephalitis in mice with intact TLR3 than in TLR3$^{-/-}$ mice. Peripheral WNV infection leads to a breakdown of the blood-brain barrier (BBB) and enhances brain infection in wild-type mice but not in TLR3$^{-/-}$ mice (50). In contrast, a protective role of the TLR3-mediated pathway in PV infection was clearly demonstrated in the present study. PV enters the CNS directly across the BBB via a PVR-independent mechanism (52) and from the neuromuscular junction via retrograde axonal transport (31–33). Because PV originally possesses two entry pathways into the CNS, the generation of a new entry pathway, even if it did occur, might not increase its deteriorative effect.

Interestingly, protective roles of the TLR3-mediated pathway have been reported for group B coxsackievirus (30, 41, 42), human rhinovirus (49), and EMCV (11) infections. Riad et al. (41) demonstrated that TRIF$^{-/-}$ mice showed severe myocarditis after CVB3 infection and IFN-β treatment improved virus control and reduced cardiac inflammation. Richer et al. (42) reported that TLR3$^{-/-}$ mice produced reduced proinflammatory mediators and were unable to control CVB4 replication at the early stages of infection, resulting in severe cardiac damage. They also showed that adoptive transfer of wild-type macrophages into TLR3$^{-/-}$ mice challenged with CVB4 resulted in greater survival, suggesting the importance of the TLR3-mediated pathway in the macrophage. Negishi et al. (30) reported that TLR3$^{-/-}$ mice showed vulnerability to CVB3 and that TLR3 signaling is linked to the activation of the type II IFN system. Since CVB3 does not induce robust type I IFNs, they suggested that the TLR3 type II IFN pathway serves as an "ace in the hole" in infections with such viruses. PV is similar to CVB3 because type I IFN production is low. However, in our preliminary experiments on PV infection in IFN-$\gamma^{-/-}$ PVR-tg mice, type II IFN did not make a significant contribution to the pathogenesis of PV. Taken together, these results suggest a critical role for the TLR3-mediated pathway, but the precise mechanisms leading to host protection are still controversial and the downstream events of TLR3 signaling after picornavirus infection remain to be elucidated.

Because the above-mentioned viruses are picornaviruses, picornavirus RNA may be easily detected by TLR3. There may be a common RNA structure in the genome or in the replication intermediates of these viruses that is detected by TLR3. Alternatively, picornaviral RNA may replicate in a compartment in which TLR3 can easily access the replicating dsRNA. To investigate these hypotheses, identification of the cells responsible for IFN production is an important step. Oshiumi et al. demonstrated that splenic CD8α^+ CD11c$^+$ cells, bone marrow-derived macrophages, and DCs are able to elicit IFN in response to PV infection (35). Further studies using this virus-cell system will elucidate the molecular recognition pattern in the PV genome, the precise mechanism of PV RNA recognition in TLR3-expressing cells, and the roles of these cells in the prevention of PV dissemination in the body.

ACKNOWLEDGMENTS

We thank Takashi Fujita, Mitsutoshi Yoneyama, Hiroki Kato, Masahiro Yamamoto, Satoshi Uematsu, Seiya Yamayoshi, Akira Ainai, Hideki Hasegawa, and Takashi Kawanishi for helpful discussions and technical assistance.

This work was supported, in part, by Grants-in-Aid from the Ministry of Education, Culture, Sports, Science and Technology, Japan (Grants-in-Aid for Scientific Research on Priority Areas no. 21022053), and Grants-in-Aid for Research on Emerging and Re-emerging Infectious Diseases from the Ministry of Health, Labor and Welfare, Japan.

REFERENCES

1. **Akira S, Uematsu S, Takeuchi O.** 2006. Pathogen recognition and innate immunity. Cell **124**:783–801.
2. **Alexopoulou L, Holt AC, Medzhitov R, Flavell RA.** 2001. Recognition of double-stranded RNA and activation of NF-kappaB by Toll-like receptor 3. Nature **413**:732–738.
3. **Barral PM, et al.** 2007. MDA-5 is cleaved in poliovirus-infected cells. J. Virol. **81**:3677–3684.
4. **Bodian D.** 1959. Poliomyelitis: pathogenesis and histopathology, p 479–518. *In*Rivers TM, Horsfall FL, Jr (ed), Viral and rickettsial infections of man, vol 3. J. B. Lippincott, Philadelphia, PA.
5. **Cella M, et al.** 1999. Plasmacytoid monocytes migrate to inflamed lymph nodes and produce large amounts of type I interferon. Nat. Med. **5**:919–923.
6. **Choe SS, Dodd DA, Kirkegaard K.** 2005. Inhibition of cellular protein secretion by picornaviral 3A proteins. Virology **337**:18–29.
7. **Colonna M, Trinchieri G, Liu YJ.** 2004. Plasmacytoid dendritic cells in immunity. Nat. Immunol. **5**:1219–1226.
8. **Diebold SS, Kaisho T, Hemmi H, Akira S, Reis e Sousa C.** 2004. Innate antiviral responses by means of TLR7-mediated recognition of single-stranded RNA. Science **303**:1529–1531.
9. **Edelmann KH, et al.** 2004. Does Toll-like receptor 3 play a biological role in virus infections? Virology **322**:231–238.
10. **Gitlin L, et al.** 2006. Essential role of mda-5 in type I IFN responses to polyriboinosinic:polyribocytidylic acid and encephalomyocarditis picornavirus. Proc. Natl. Acad. Sci. U. S. A. **103**:8459–8464.
11. **Hardarson HS, et al.** 2007. Toll-like receptor 3 is an essential component of the innate stress response in virus-induced cardiac injury. Am. J. Physiol. Heart Circ. Physiol. **292**:H251–H258.
12. **Hemmi H, et al.** 2002. Small anti-viral compounds activate immune cells via the TLR7 MyD88-dependent signaling pathway. Nat. Immunol. **3**:196–200.
13. **Hoebe K, et al.** 2003. Identification of Lps2 as a key transducer of MyD88-independent TIR signalling. Nature **424**:743–748.
14. **Holland JJ.** 1961. Receptor affinities as major determinants of enterovirus tissue tropisms in humans. Virology **15**:312–326.
15. **Holland JJ, Mc LL, Syverton JT.** 1959. Mammalian cell-virus relationship. III. Poliovirus production by non-primate cells exposed to poliovirus ribonucleic acid. Proc. Soc. Exp. Biol. Med. **100**:843–845.
16. **Holland JJ, McLaren LC, Syverton JT.** 1959. The mammalian cell-virus relationship. IV. Infection of naturally insusceptible cells with enterovirus ribonucleic acid. J. Exp. Med. **110**:65–80.
17. **Hornung V, et al.** 2006. 5′-Triphosphate RNA is the ligand for RIG-I. Science **314**:994–997.
18. **Hsiung GD, Black FL, Henderson JR.** 1964. Susceptibility of primates to viruses in relation to taxonomic classification, p 1–23. *In*Buettner-Jaenusch J (ed), Evolutionary and genetic biology of primates, vol 2. Academic Press, New York, NY.
19. **Ida-Hosonuma M, et al.** 2005. The alpha/beta interferon response controls tissue tropism and pathogenicity of poliovirus. J. Virol. **79**: 4460–4469.
20. **Ida-Hosonuma M, et al.** 2003. Host range of poliovirus is restricted to simians because of a rapid sequence change of the poliovirus receptor gene during evolution. Arch. Virol. **148**:29–44.
21. **Kato H, et al.** 2005. Cell type-specific involvement of RIG-I in antiviral response. Immunity **23**:19–28.
22. **Kato H, et al.** 2008. Length-dependent recognition of double-stranded ribonucleic acids by retinoic acid-inducible gene-I and melanoma differentiation-associated gene 5. J. Exp. Med. **205**:1601–1610.
23. **Kato H, et al.** 2006. Differential roles of MDA5 and RIG-I helicases in the recognition of RNA viruses. Nature **441**:101–105.
24. **Koike S, et al.** 1992. A second gene for the African green monkey poliovirus receptor that has no putative N-glycosylation site in the functional N-terminal immunoglobulin-like domain. J. Virol. **66**:7059–7066.

25. **Koike S, Nomoto A.** 2010. Poliomyelitis, p 339–351. *In*Ehrenfeld E, Domingo E, Roos RP (ed), The picornaviruses. ASM Press, Washington, DC.
26. **Koike S, et al.** 1991. Transgenic mice susceptible to poliovirus. Proc. Natl. Acad. Sci. U. S. A. **88**:951–955.
27. **Kramer M, et al.** 2008. Phagocytosis of picornavirus-infected cells induces an RNA-dependent antiviral state in human dendritic cells. J. Virol. 82:2930–2937.
28. **Matsumoto M, et al.** 2003. Subcellular localization of Toll-like receptor 3 in human dendritic cells. J. Immunol. **171**:3154–3162.
29. **Matsumoto M, Oshiumi H, Seya T.** 2011. Antiviral responses induced by the TLR3 pathway. Rev. Med. Virol. **21**:67–77.
30. **Negishi H, et al.** 2008. A critical link between Toll-like receptor 3 and type II interferon signaling pathways in antiviral innate immunity. Proc. Natl. Acad. Sci. U. S. A. **105**:20446–20451.
31. **Ohka S, et al.** 2004. Receptor (CD155)-dependent endocytosis of poliovirus and retrograde axonal transport of the endosome. J. Virol. **78**: 7186–7198.
32. **Ohka S, et al.** 2009. Receptor-dependent and -independent axonal retrograde transport of poliovirus in motor neurons. J. Virol. **83**:4995–5004.
33. **Ohka S, Yang WX, Terada E, Iwasaki K, Nomoto A.** 1998. Retrograde transport of intact poliovirus through the axon via the fast transport system. Virology **250**:67–75.
34. **Oshiumi H, Matsumoto M, Funami K, Akazawa T, Seya T.** 2003. TICAM-1, an adaptor molecule that participates in Toll-like receptor 3-mediated interferon-beta induction. Nat. Immunol. **4**:161–167.
35. **Oshiumi H, et al.** 12 October 2011, posting date. The TLR3-TICAM-1 pathway is mandatory for innate immune responses to poliovirus infection. J. Immunol. [Epub ahead of print.] doi:10.4049/jimmunol.1101503.
36. **Pichlmair A, et al.** 2006. RIG-I-mediated antiviral responses to single-stranded RNA bearing 5′-phosphates. Science **314**:997–1001.
37. **Pichlmair A, et al.** 2009. Activation of MDA5 requires higher-order RNA structures generated during virus infection. J. Virol. **83**:10761–10769.
38. **Racaniello VR.** 2007. Picornaviridae: the viruses and their replication, p 795–838. *In*Knipe DM, Howley PM (ed), Fields virology, 5th ed. Lippincott Williams & Wilkins, Philadelphia, PA.
39. **Rebsamen M, Meylan E, Curran J, Tschopp J.** 2008. The antiviral adaptor proteins Cardif and Trif are processed and inactivated by caspases. Cell Death Differ. **15**:1804–1811.
40. **Ren RB, Costantini F, Gorgacz EJ, Lee JJ, Racaniello VR.** 1990. Transgenic mice expressing a human poliovirus receptor: a new model for poliomyelitis. Cell **63**:353–362.
41. **Riad A, et al.** 2011. TRIF is a critical survival factor in viral cardiomyopathy. J. Immunol. **186**:2561–2570.
42. **Richer MJ, Lavallee DJ, Shanina I, Horwitz MS.** 2009. Toll-like receptor 3 signaling on macrophages is required for survival following coxsackievirus B4 infection. PLoS One **4**:e4127.
43. **Schröder M, Bowie AG.** 2005. TLR3 in antiviral immunity: key player or bystander? Trends Immunol. **26**:462–468.
44. **Schulz O, et al.** 2005. Toll-like receptor 3 promotes cross-priming to virus-infected cells. Nature **433**:887–892.
45. **Shiroki K, et al.** 1995. A new *cis*-acting element for RNA replication within the 5′ noncoding region of poliovirus type 1 RNA. J. Virol. **69**: 6825–6832.
46. **Takeuchi O, Akira S.** 2009. Innate immunity to virus infection. Immunol. Rev. **227**:75–86.
47. **Takeuchi O, Akira S.** 2008. MDA5/RIG-I and virus recognition. Curr. Opin. Immunol. **20**:17–22.
48. **Takeuchi O, Akira S.** 2007. Recognition of viruses by innate immunity. Immunol. Rev. **220**:214–224.
49. **Wang Q, et al.** 2009. Role of double-stranded RNA pattern recognition receptors in rhinovirus-induced airway epithelial cell responses. J. Immunol. **183**:6989–6997.
50. **Wang T, et al.** 2004. Toll-like receptor 3 mediates West Nile virus entry into the brain causing lethal encephalitis. Nat. Med. **10**:1366–1373.
51. **Yamamoto M, et al.** 2003. Role of adaptor TRIF in the MyD88-independent Toll-like receptor signaling pathway. Science **301**:640–643.
52. **Yang WX, et al.** 1997. Efficient delivery of circulating poliovirus to the central nervous system independently of poliovirus receptor. Virology **229**:421–428.
53. **Yoneyama M, et al.** 2004. The RNA helicase RIG-I has an essential function in double-stranded RNA-induced innate antiviral responses. Nat. Immunol. **5**:730–737.
54. **Yoshikawa T, et al.** 2006. Role of the alpha/beta interferon response in the acquisition of susceptibility to poliovirus by kidney cells in culture. J. Virol. **80**:4313–4325.
55. **Yousefi S, Escobar MR, Gouldin CW.** 1985. A practical cytopathic effect/dye-uptake interferon assay for routine use in the clinical laboratory. Am. J. Clin. Pathol. **83**:735–740.

RESEARCH PAPER

OncoImmunology 1:5, 581–592; August 2012; © 2012 Landes Bioscience

Cross-priming for antitumor CTL induced by soluble Ag + polyI:C depends on the TICAM-1 pathway in mouse CD11c$^+$/CD8α^+ dendritic cells

Masahiro Azuma, Takashi Ebihara,† Hiroyuki Oshiumi, Misako Matsumoto and Tsukasa Seya*

Department of Microbiology and Immunology; Hokkaido University Graduate School of Medicine; Sapporo, Japan

†Current affiliation: Howard Hughes Medical Institute; Washington University School of Medicine; St. Louis, MO USA

Keywords: cross-presentation, dendritic cell, TLR3, TICAM-1 (TRIF), tumoricidal CTL

Abbreviations: APC, antigen-presenting cells; CTL, cytotoxic T lymphocytes; DAMP, damage-associated molecular pattern; DC, dendritic cells; IFN, interferon; IPS-1, IFNβ promoter stimulator-1; MDA5, melanoma differentiation associated gene 5; Mf, macrophages; NK, natural killer; OVA, ovalbumin; PAMP, pathogen-associated molecular pattern; PRR, pattern-recognition receptors; PV, poliovirus; RIG-I, retinoic acid inducible gene-1; SL8, an OVA tetramer; TICAM-1, Toll-IL-1 receptor homology domain-containing molecule-1; TLR, Toll-like receptor; WT, wild-type

PolyI:C is a nucleotide pattern molecule that induces cross-presentation of foreign Ag in myeloid dendritic cells (DC) and MHC Class I-dependent proliferation of cytotoxic T lymphocytes (CTL). DC (BM or spleen CD8α$^+$) have sensors for dsRNA including polyI:C to signal facilitating cross-presentation. Endosomal TLR3 and cytoplasmic RIG-I/MDA5 are reportedly responsible for polyI:C sensing and presumed to deliver signal for cross-presentation via TICAM-1 (TRIF) and IPS-1 (MAVS, Cardif, VISA) adaptors, respectively. In fact, when tumor-associated Ag (TAA) was simultaneously taken up with polyI:C in DC, the DC cross-primed CTL specific to the TAA in a syngenic mouse model. Here we tested which of the TICAM-1 or IPS-1 pathway participate in cross-presentation of tumor-associated soluble Ag and retardation of tumor growth in the setting with a syngeneic tumor implant system, EG7/C57BL6, and exogenously challenged soluble Ag (EG7 lysate) and polyI:C. When EG7 lysate and polyI:C were subcutaneously injected in tumor-bearing mice, EG7 tumor growth retardation was observed in wild-type and to a lesser extent IPS-1$^{-/-}$ mice, but not TICAM-1$^{-/-}$ mice. IRF-3/7 were essential but IPS-1 and type I IFN were minimally involved in the polyI:C-mediated CTL proliferation. Although both TICAM-1 and IPS-1 contributed to CD86/CD40 upregulation in CD8α$^+$ DC, H2K^b-SL8 tetramer and OT-1 proliferation assays indicated that OVA-recognizing CD8 T cells predominantly proliferated in vivo through TICAM-1 and CD8α$^+$ DC is crucial in ex vivo analysis. Ultimately, tumor regresses > 8 d post polyI:C administration. The results infer that soluble tumor Ag induces tumor growth retardation, i.e., therapeutic potential, if the TICAM-1 signal coincidentally occurs in CD8α$^+$ DC around the tumor.

Introduction

Cytotoxic T lymphocytes (CTL) and natural killer (NK) cells are two major effectors for antitumor cellular immunity. These effectors are driven through activation of dendritic cells (DC) and/or macrophages (Mf), which is mediated by pattern-recognition receptors (PRRs) for the recognition of microbial patterns.[1,2] Antigen (Ag) presentation and upregulation of NK cell-activating ligands are major events induced in DC/Mf in response to PRRs, which link to evoking CTL- and NK-antitumor immunity, respectively. The immune-potentiating function of specific components of the classical adjuvants are largely attributable to the ligand activity of PRRs (CpG DNA/TLR9, polyI:C/TLR3, monophosphoryl lipid (MPL) A/TLR4, Pam2/TLR2, etc.).[3] That is, the DC/Mf competent to drive effectors are generated through PRR signal in inflammatory nest where affected cells and recruited immune cells encounter exogenous or endogenous PRR ligands. Since studying the functional properties of PRRs in tumor immunity is on the way using a variety of possible ligands and cell biological analyses, immune responses reflecting the total adjuvant potential around Ag-presenting cells (APC) in local inflammatory nests are not always elucidated even in mice.

RNA-sensing PRR pathways, including TLR3-TICAM-1, TLR7-MyD88 and RIG-I/MDA5-IPS-1 participate in driving Type I IFN induction and cellular immunity in DC subsets.[1,4,5] Type I IFN and the IFNAR pathway in DC and other cells reportedly evoke and amplify T cell immunity.[5,6] TLR7 resides exclusively in plasmacytoid DC[7] whereas TLR3 mainly exists in

*Correspondence to: Tsukasa Seya; Email: seya-tu@pop.med.hokudai.ac.jp
Submitted: 02/04/12; Revised: 03/02/12; Accepted: 03/02/12
http://dx.doi.org/10.4161/onci.19893

myeloid DC/Mf and epithelial cells.[8] They are localized on the membrane of the endosome and deliver the signal via their adaptors, MyD88 and TICAM-1.[7,8] RIG-I and MDA5 are ubiquitously distributed to a variety of mouse cells and signal the presence of cytoplasmic viral products through IPS-1.[9] Thus, TLR3 and RIG-I/MDA5 are candidates associated with DC maturation to drive effector cells.[10] Indeed, viral dsRNA analog, polyI:C, is a representative ligand for TLR3 and MDA5 and induces polyI:C-mediated DC-NK reciprocal activation.[11,12] These are also true in human DC.[13]

The point of this study is by which pathway antitumor CTL are induced for tumor regression in a mouse tumor-implant model. It has been postulated that DC present exogenous tumor Ag to the MHC Class I-restricted Ag-presentation pathway and proliferate CD8 T cells specific to the extrinsic Ag. When tumor cells provide soluble and insoluble exogenous Ag, this Class I Ag presentation occurs mostly TAP/proteasome-dependent, suggesting the pathway partly sharing with that for endogenous Ag presentation. This DC's ability to deliver exogenous Ag to the pathway for MHC Class I-restricted Ag presentation has been described as cross-presentation.[14] DC cross-presentation leads to the cross-priming and proliferation of Ag-specific CD8 T cells in vivo and in vitro.[14-18] A variety of PAMP[15,16] and intrinsic DAMP[17] as well as other factors including Type I IFN,[5,18] $CD4^+$ T cells[19] and NKT cells[20] augment cross-priming in tumor-bearing mice. However, by what molecular mechanism polyI:C enhances CTL induction in tumor-bearing mice remains largely unsettled.

Here, we made an EG7 tumor-implant mouse system and treated the mice with s.c.-injected ovalbumin (OVA)-containing cell lysates (Ag) and polyI:C. Spleen $CD8\alpha^+$ DC turn CTL-inducible when stimulated with Ag and polyI:C. In either case of s.c., i.p., or i.v. injection of polyI:C, the TLR3/TICAM-1 pathway predominantly participates in $CD8\alpha^+$ DC cross-priming and antitumor CTL induction. Earlier studies using non-tumor models, suggested that both TLR3 and MDA5 appeared to participate in polyI:C-dependent CTL induction.[21] TLR3 is predominantly involved in primary Ag response and Th1 skewing,[22] while MDA5 participates in secondary Ag response.[23] Importance of TLR3 in induction of cross-priming was first suggested by Schulz et al., who used OVA/polyI:C-loaded or virus-infected xenogenic (Vero) cells and mouse DC.[16] Here we demonstrate that the antitumor polyI:C activity is sustained by the TICAM-1 pathway in any route of injection in tumor-implant mice: antitumor CTL responses are mostly abrogated in TICAM-$1^{-/-}$ but not IPS-$1^{-/-}$ mice.

Results

Properties of EG7 tumor with high MHC in tumor-loading mice. The properties of the EG7 line we used are consistent with those reported previously.[24,25] It expressed high MHC Class I (H2-Kb) and no Qa-1b or Rae-1 (**Fig. S1**). The expression levels of these proteins were barely changed before and after implantation of EG7 cells into mice. Cell viability was not affected by in vitro stimulation with polyI:C only (**Fig. S1B**). However, a batch-to-batch difference of cell viability may have affected the rate of tumor growth in each mouse tumor-implant experiment.

$CD8^+$ T cells are responsible for tumor retardation by polyI:C. EG7 cells (2×10^6) were inoculated into the back of C57BL/6 (WT), and the indicated reagents were subcutaneously (s.c.) injected around the EG7 tumor (**Fig. 1A**). Growth retardation of tumor was observed by treatment with polyI:C or polyI:C plus EG7 lysate (**Fig. 1A**). EG7 lysate only had no effect on tumor regression. When $CD8\beta^+$ T cells were depleted before EG7 lysate/polyI:C treatment, polyI:C-mediated tumor growth suppression was cancelled (**Fig. 1A**), suggesting the participation of CD8 T cells in tumor growth suppression. The therapeutic potential of polyI:C appeared to be more reproducible in the presence of EG7 lysate than in the absence, judged from the increases of activated $CD8^+$ T cells (**Fig. 1B**) and cytotoxic activity (**Fig. 1C**) of LN T cells isolated from the mice sacrificed after the last therapy. Yet, the EG7 Ag could be more or less supplied from the implant tumor. $NK1.1^+$ cells did not participate in this EG7 tumor regression in this setting (data not shown).

Since EG7 lysate contains OVA, OVA-specific T cells in draining LN and spleen of the WT mice were counted by tetramer assay after the last therapy (**Fig. S2A and B**). The numbers of tetramer-positive cells were prominently increased in LN and spleen in mice with EG7 lysate and polyI:C. We confirmed the importance of simultaneous administration of Ag plus polyI:C for OVA-specific CTL induction as in **Figure S2C**, where pure Ag (OVA) was used instead of EG7 lysate for immunotherapy. The polyI:C adjuvant function appeared to be more efficient in the mixture of pure Ag than in polyI:C alone. Tumor regression (**Fig. S2C**) and OVA-specific CTL induction (**Fig. S2D**) were clearly observed in this additional experiment. To obtain reproducible data, we employed the EG7 lysate/polyI:C combination therapy as follows.

IFN-inducing pathways are involved in PolyI:C-derived EG7 growth retardation. We next inoculated EG7 cells (2×10^6) into the back of C57BL/6 (WT), TICAM-$1^{-/-}$, IPS-$1^{-/-}$, or TICAM-1/IPS-1 double-deficient (DKO) mice (**Fig. 2**). We s.c. administered EG7 lysate with or without polyI:C around the tumor. The EG7 lysate was the soluble fraction of EG7 which removed insoluble debris by centrifugation. The EG7 lysate contained unprecipitated micro-debris and soluble Ag. No other emulsified reagent was added for immunization. Thus, the adjuvant function of polyI:C per se is reflected in the tumor growth, although polyI:C had to be injected into mice twice a week. Retardation of tumor growth was observed $>$ 8 d after immunization with EG7 lysate + polyI:C in WT mice, though no growth retardation without polyI:C (**Fig. 2A**). The polyI:C-mediated tumor growth suppression was largely abrogated in TICAM-$1^{-/-}$ (**Fig. 2B**) and to a lesser extent in IPS-$1^{-/-}$ mice (**Fig. 2C**), and completely in TICAM-1/IPS-1 DKO mice (**Fig. 2D**). Hence, TICAM-1 plays an important role in inducing polyI:C-mediated tumor growth retardation in the s.c. setting we employed.

CD8 T cell activation induced by the TICAM-1 pathway. CD8 T cell activation in the inguinal LN was tested with polyI:C + EG7 lysate in EG7 tumor-bearing mice using CD69 as

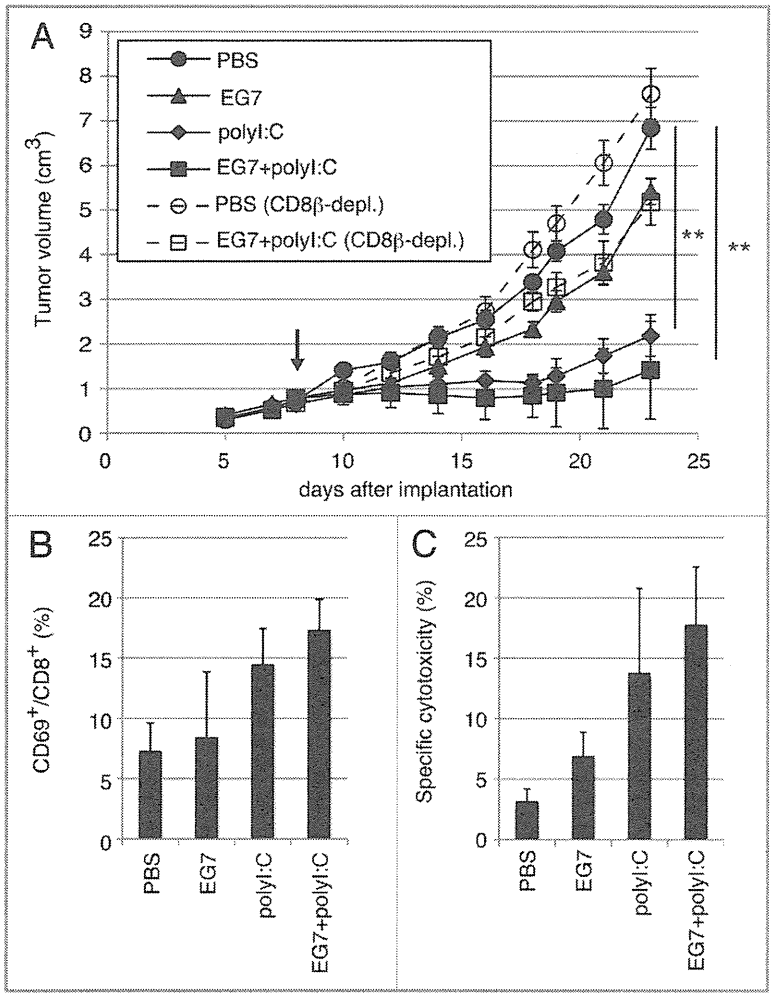

Figure 1. PolyI:C induces CTL-mediated tumor regression. (A) WT mice were challenged with EG7 cells and were treated with PBS (●), EG7 lysates (▲), polyI:C (◆) and EG7 lysates + polyI:C (■). The adjuvant therapy was started at the time indicated by the arrow and the indicated reagents injected twice per week. One of the two PBS groups (○) and one of the two EG7 lysates + polyI:C groups (□) were treated with anti-CD8β ascites in order to deplete $CD8^+$ T cells once a week. Each group had 3–5 mice. (B) Draining inguinal LNs were harvested 24 h after the last treatment and the proportion of CD69-expressing $CD8^+$ cells were counted. (C) LN cells were co-cultured with MMC-treated EG7 cells for 3 d and subjected to ^{51}Cr release assay to evaluate CTL activity. E/T = 50. All error bars used in this figure show ± SEM. Data are representative of two independent experiments. One-way analysis of variance (ANOVA) with Bonferroni's test was performed to analyze statistical significance. **, $p < 0.01$.

an activating marker. Twenty-four hours after the last polyI:C + EG7 sec.c. treatment, cells were harvested from the LN excised (**Fig. 3A**). FACS profiles of total cells from each mouse group are shown in **Fig. S3**. By combination therapy with EG7 lysate and polyI:C, T cells were activated in WT and IPS-$1^{-/-}$ mice, but the proportion of CD8 T cells was not affected by the therapy (**Fig. S4A**). Under the same conditions, T cells were barely activated in TICAM-$1^{-/-}$ mice in response to polyI:C (**Fig. 3A**). The proportion of $CD69^+$ cells are indicated in **Figure 3B**. IL-2 (**Fig. 3C**) and IFNγ (**Fig. S4B**) were highly induced in the WT and IPS-$1^{-/-}$ LN cells, while they were not induced in TICAM-$1^{-/-}$ or DKO cells. IFNγ levels were upregulated only in polyI:C-treated tumor-bearing mice, although the WT > IPS-$1^{-/-}$ profile for IFNγ production was reproducibly observed (**Fig. S4B**).

In vivo proliferation of CD8 T cells judged by tetramer assay and IFNγ induction. We next tested whether i.p. injection of polyI:C plus OVA induces CTL proliferation. PolyI:C and OVA were i.p. injected into mice and the polyI:C-dependent cross-priming of CD8 T cells were examined using the OVA tetramer assay. OVA-specific CD8 T cells were clonally proliferated in WT and IPS-$1^{-/-}$ mice, but not in TICAM-1/IPS-1 DKO and IRF-$3/7^{-/-}$ mice (**Fig. 4A**). Proliferation of OVA-specific CD8 T cells were severely suppressed in TICAM-$1^{-/-}$ mice (**Fig. 4A**), suggesting that polyI:C-mediated cross-priming of CD8 T cells largely depends on the TICAM-1 pathway followed by IRF-3/7 activation in the i.p. route. The results were reproduced in additional experiments using more mice (**Fig. 4B**) and TLR$3^{-/-}$ mice (**Fig. S5A and B**). The polyI:C cytokine response, where IFNα is IPS-1-dependent while IL-12p40 is TICAM-1-dependent, was also confirmed in serum level by polyI:C i.p. injection (**Fig. S5E**). Specific induction of IFNγ (**Fig. 4C**) was also observed in parallel with the results of **Figure 4A**.

Whether or not i.v. injection of polyI:C plus OVA induces Ag-specific CTL and cytotoxicity was next checked. OVA-specific OT-1 proliferation and cytotoxicity (**Fig. 4D and E**) were observed in in vivo analyses of WT and IPS-$1^{-/-}$ CD8 T cells but not of TICAM-$1^{-/-}$, TICAM-1/IPS-1 DKO, and IRF-$3/7^{-/-}$ mice in the i.v. setting.

Since TICAM-1 is the adaptor for TLR3 as well as cytoplasmic helicases,[24] we confirmed the level of cross-priming being decreased in TLR$3^{-/-}$ mice and an expected result was obtained (**Fig. S5A and B**). Furthermore, in IFNAR$^{-/-}$ mice, OVA-specific CTL induction was slightly reduced compared with that in WT mice, but higher than in TICAM-$1^{-/-}$ mice (**Fig. S5C and D**). Hence, in vivo cross-presentation induced by polyI:C mostly depends on the TLR3-TICAM-1 pathway followed by transcriptional regulation by IRF-3/7 in any administration route, and is further promoted by Type I IFN presumably produced by the stromal cells through the IPS-1 pathway.[26]

IPS-1 induces DC maturation but not cross-priming in vivo. Spleen DC maturation by i.v.-injected polyI:C was tested ex vivo using $CD8\alpha^+$ DC and $CD8\alpha^-$ DC isolated from WT or KO mice with no tumor as indicated in **Figure 5A**. The maturation markers CD86 and CD40 were upregulated on both $CD8\alpha^+$ and $CD8\alpha^-$

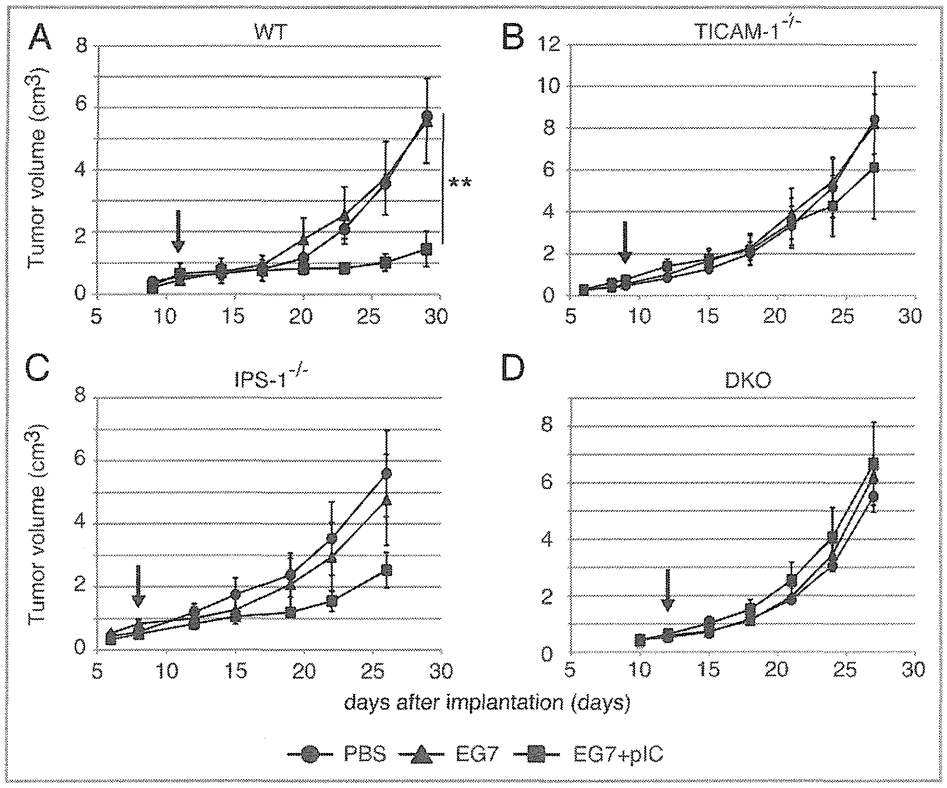

Figure 2. PolyI:C-induced tumor retardation is dependent on the TICAM-1 pathway. Antitumor effect of polyI:C on various KO mice were evaluated by using in vivo mouse tumor implant model. EG7 cells were inoculated to WT (A), TICAM-1$^{-/-}$ (B), IPS-1$^{-/-}$ (C) and DKO mice (D) on day 0. PBS (●), EG7 lysates (▲) or EG7 lysates + polyI:C (■) were s.c. administered around the tumor. The adjuvant therapies were started at the time indicated by the arrows and injected twice per week. Each group have 3–4 mice and error bar shows ± SEM. Data are representative of two independent experiments. **, $p < 0.01$

DC from WT mice when they were stimulated with OVA and polyI:C. Treatment of DC with OVA only did not induce upregulation of CD86 and CD40. Although the expression levels of CD86 and CD40 were a little less in CD8α$^+$ and CD8α$^-$ DC from TICAM-1$^{-/-}$ or IPS-1$^{-/-}$ mice than those from WT mice, both CD86 and CD40 were sufficiently upregulated even in the abrogation of either one pathway in polyI:C-injected mice. The CD86 and CD40 shifts were completely abolished in DKO mice (**Fig. 5A**). Thus, the TICAM-1 pathway participates in both potent co-stimulation and cross-priming, while the IPS-1 pathway mainly participates only in integral co-stimulation in myeloid DC.

We next assessed in vitro proliferation of OT-1 cells. CD8α$^+$ and CD8α$^-$ DC were prepared from PBS, polyI:C, OVA and OVA/polyI:C-treated mice, and mixed in vitro with CFSE-labeled OT-1 cells. WT, TICAM-1$^{-/-}$ and IPS-1$^{-/-}$ mice were used for this study. OT-1 proliferation was observed with CD8α$^+$ DC but not CD8α$^-$ DC when OVA + polyI:C was injected (**Fig. 5B**). Furthermore, the OT-1 proliferation barely occurred in the mixture containing TICAM-1$^{-/-}$ CD8α$^+$ DC. Thus, OT-1 proliferation is triggered by the TICAM-1 pathway in CD8α$^+$ DC. Again, IPS-1 had almost no effect on OT-1 proliferation with CD8α$^+$ DC in this setting. In the mixture, IFNγ was produced in the supernatants of WT and IPS-1$^{-/-}$ CD8α$^+$ DC but not TICAM-1$^{-/-}$ DC by stimulation with OVA + polyI:C (**Fig. 5C**). No IFNγ was produced in the supernatants of CD8α$^-$ DC even from WT mice, which results are in parallel with those of OT-1 proliferation. In any case irrespective of tumor-bearing or not, Ag, polyI:C and the TICAM-1 pathway are mandatory for CD8α$^+$ DC to cross-prime and proliferate OVA-specific CD8 T cells.

We checked the TICAM-1- or IPS-1-specific gene expressions related to Type I IFN and MHC Class I presentation using genechip and qPCR (**Fig. S6**). PolyI:C-mediated upregulation of *Tap1*, *Tap2* and *Tapbp* messages diminished in TICAM-1$^{-/-}$ BMDC (**Fig. S6A**). The levels of these genes were hardly affected in IPS-1$^{-/-}$ BMDC (data not shown). PolyI:C-mediated upregulation was observed with MDA5 (*Ifih1*) in CD8α$^-$ and CD8α$^+$ DCs (**Fig. S6B**). Surprisingly, other factors including TLR3, TICAM-1 and MAVS messages were all downregulated in response to polyI:C in CD8α$^+$ DC (**Fig. S6B**), for the reason as yet unknown.

Effect of TLR3-mediated IFN-inducing pathway on anti-tumor CTL induction. PolyI:C is a dsRNA analog capable of incorporating into the endosome and cytoplasm by exogenous administration in vitro.[27,28] However, no evidence has been proposed that polyI:C is internalized into the endosome of

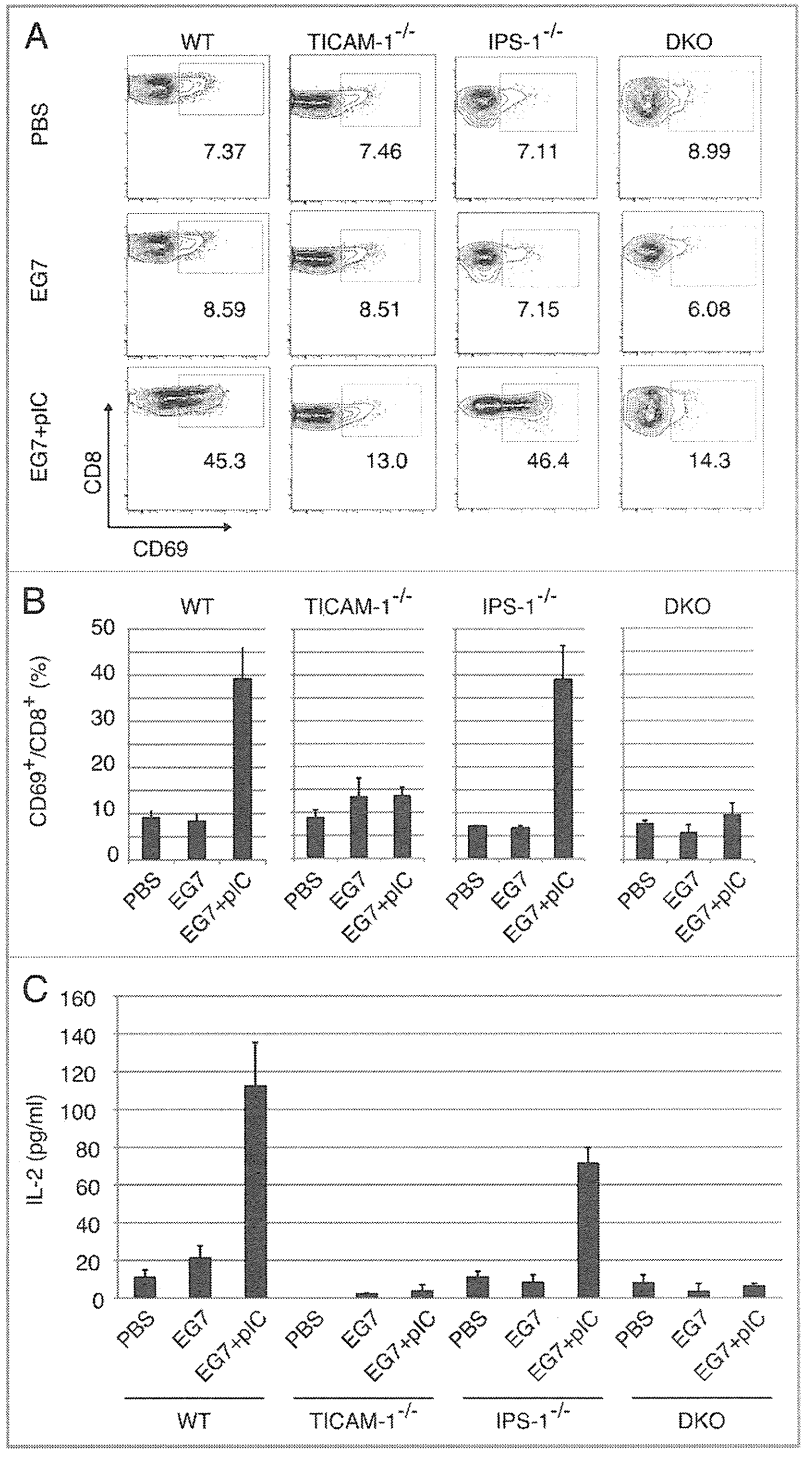

Figure 3. CD8 T cells in the draining LNs are activated through the TICAM-1 pathway by polyI:C. Draining inguinal LNs were harvested from tumor-bearing mice 24 h after the last treatment. LN cells were stained with CD3ε, CD8α and CD69, and the cells gated on $CD3\varepsilon^{+}CD8\alpha^{+}$ are shown (A). Spleen cells in each group of mice were stained separately, the CD8 levels in gated cells being variably distributed in FACS analyses. The average frequency of activated CD8 T cells defined by CD69 expression is shown (B). Alternatively, LN cells from the indicated mice were cultured for further 3 d in vitro and IL-2 production was measured by CBA assay (C).

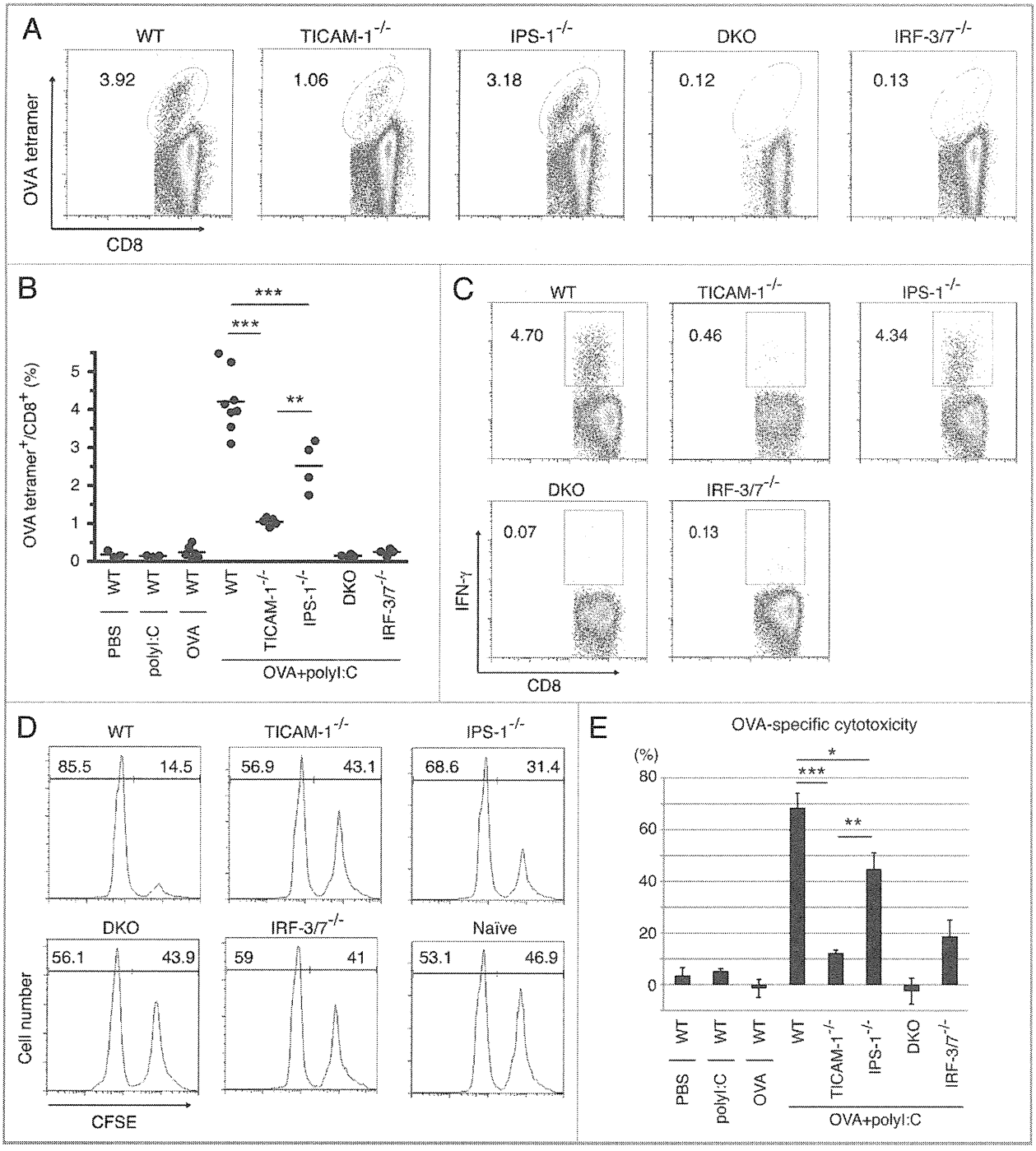

Figure 4. TICAM-1 and IRF-3/7 are essential for polyI:C-induced antigen-specific CTL expansion. WT, TICAM-1$^{-/-}$, IPS-1$^{-/-}$, TICAM-1/IPS-1 DKO and IRF-3/7$^{-/-}$ mice were i.p. administered with the combination of OVA and polyI:C. After 7days, splenocytes were harvested and stained with CD8α and OVA tetramer (A). The average percentages of OVA-specific CTL are shown (B). Alternatively, splenocytes were cultured in vitro in the presence of SL8 for 8 h and IFNγ production was measured by intracellular cytokine staining (C). To assess the killing activity, in vivo CTL assay was performed. The combinations of OVA and polyI:C were administered i.v. to each group of mice and 5 d later, cytotoxicity was measured (D). The data shown are collaborate or representative of at least three independent experiments. One-way analysis of variance (ANOVA) with Bonferroni's test was performed to analyze statistical significance. *, $p < 0.05$; **, $p < 0.01$; ***, $p < 0.001$.

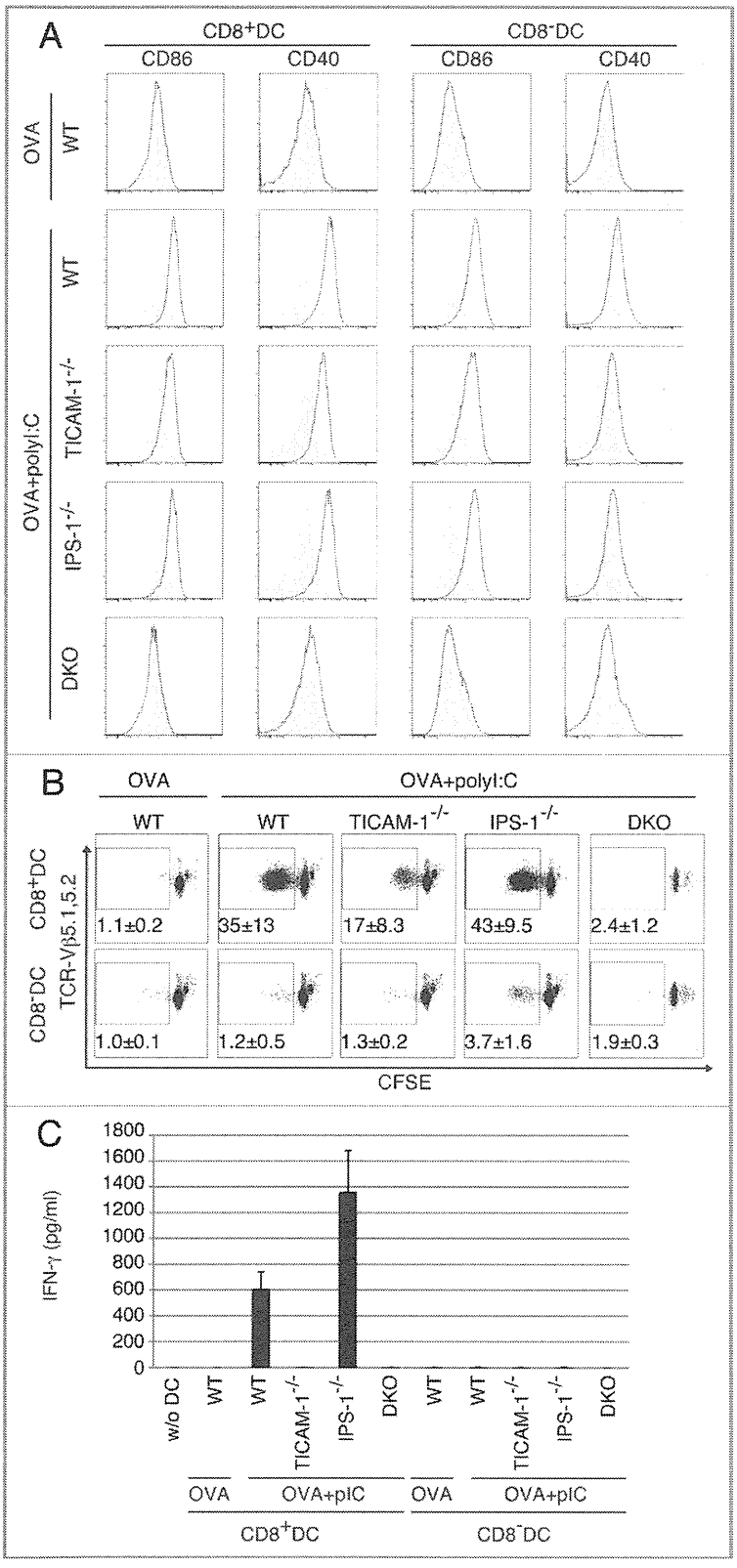

Figure 5. TICAM-1 in CD8α⁺ DC is more important than IPS-1 in polyI:C-induced cross-priming. OVA and polyI:C were administered i.v. and 4 h later, CD8α⁺ and CD8α⁻ DC were isolated from the spleen. CD86 and CD40 expressions were determined by FACS (A). Filled gray and black line show isotype control and target expression, respectively. Alternatively, CD8α⁺ and CD8α⁻ DC were co-cultured with CFSE-labeled RAG2$^{-/-}$/OT-1 T cells for 3 d. The cross-priming activity of each DC subset was determined with sequential dilution of CFSE (B) and IFNγ production (C). IFNγ was measured by CBA assay. The data shown are representative of two independent experiments. Err bar shows SD.

CD8α⁺ DC where TLR3 is expressed in vivo. Peritoneal (PEC) Mf and bone marrow-derived DC[22] usually phagocytoze polyI:C and deliver them into the endosome. In mouse CD8α⁺ DC direct internalization of polyI:C has remain unproven. Using labeled polyI:C and anti-mouse TLR3 mAb, 11F8,[22] we checked whether the exogenously-added polyI:C encountered with TLR3 in CD8α⁺ DC in vitro. TLR3 (green) was merged with TexasRed-polyI:C 30–120 min after polyI:C stimulation in the culture (**Fig. 6A**). The quantities of CD8α⁺ and CD8α⁻ DC where FITC-polyI:C was incorporated were determined by FACS analysis (**Fig. 6B**). Thus, the process by which polyI:C injected reaches the endosomal TLR3 is delineated in the CD8α⁺ DC.

Discussion

PolyI:C is an analog of virus dsRNA, and acts as a ligand for TLR3 and RIG-I/MDA5. PolyI:C has been utilized as an adjuvant for enhancement of antitumor immunity for a long time.[29] However, the mechanistic background of the therapeutic potentials of polyI:C against cancer has been poorly illustrated. It induces antitumor NK activation through DC-NK cell-to-cell interaction when CD8α⁺ DC TLR3 is stimulated in the spleen.[11] Besides myeloid cells, however, some tumor cell lines express TLR3 and dsRNA targeting tumor cells may affect the growth rate of tumors,[30] where the receptor-interacting protein (RIP) pathway is involved downstream of TICAM-1.[31] Here we showed evidence that polyI:C injection facilitates maturation of TLR3-positive CD8α⁺ DC (i.e., APC) to trigger CTL induction against exogenous soluble Ags including EG7 lysate or OVA. The TICAM-1 adaptor for TLR3 and IRF-3/7 are involved in the cross-presentation signal in CD8α⁺ DC, but the molecule/mechanism downstream of TICAM-1 that governs cross-presentation remains elusive. Since most of the tumor-associated Ags (TAA) are predicted to be liberated from tumor cells